

**AIX-MARSEILLE UNIVERSITY**

**DOCTORAL SCHOOL: Physics and Material Science**

PARTENAIRES DE RECHERCHE

Laboratoire MADIREL

Submitted with the view of obtaining the degree of doctor

Discipline: Material Science

Specialty: Characterisation of porous materials

**Paul A. Iacomì**

Titre de la thèse: sous-titre de la thèse

Defended on JJ/MM/AAAA in front of the following jury:

Prénom NOM	Affiliation	Rapporteur
Prénom NOM	Affiliation	Rapporteur
Prénom NOM	Affiliation	Examineur
Prénom NOM	Affiliation	Examineur
Prénom NOM	Affiliation	Examineur
Prénom NOM	Affiliation	Directeur de thèse

National thesis number: 2017AIXM0001/001ED62



This work falls under the conditions of the Creative Commons Attribution License - No commercial use - No modification 4.0 International.

# Abstract

Abstract is here.

# Acknowledgements

Acknowledgements go here

# Contents

<b>Abstract</b>	<b>iv</b>
<b>Acknowledgements</b>	<b>v</b>
<b>1. Building a framework for adsorption data processing</b>	<b>1</b>
1.1. Introduction . . . . .	1
1.2. Physical models of adsorption . . . . .	2
1.2.1. The Henry model . . . . .	3
1.2.2. Langmuir and multi-site Langmuir model . . . . .	3
1.2.3. BET model . . . . .	6
1.2.4. Toth model . . . . .	7
1.2.5. Temkin model . . . . .	7
1.2.6. Jensen-Seaton model . . . . .	8
1.2.7. Quadratic model . . . . .	8
1.2.8. Virial model . . . . .	9
1.2.9. Vacancy solution theory models . . . . .	9
1.3. Characterisation of materials through adsorption . . . . .	10
1.3.1. Specific surface area and pore volume calculation . . . . .	11
1.3.2. Assessing porosity . . . . .	14
1.3.3. Predicting multicomponent adsorption . . . . .	19
1.4. pyGAPS overview . . . . .	21
1.4.1. Core structure . . . . .	21
1.4.2. Creation of an Isotherm . . . . .	23
1.4.3. Units . . . . .	25
1.4.4. Workflow . . . . .	25
1.4.5. Characterisation using pyGAPS . . . . .	26
1.5. Processing a large adsorption dataset . . . . .	33
1.5.1. The NIST ISODB dataset . . . . .	33
1.5.2. A comparison between surface area calculation methods . . . . .	35
1.5.3. Variability of the dataset . . . . .	36
1.6. Conclusion . . . . .	39
Bibliography . . . . .	40

<b>2. Extending bulk analysis of porous compounds through calorimetry</b>	<b>43</b>
2.1. Introduction . . . . .	43
2.2. Energetics of adsorption . . . . .	44
2.2.1. Forces involved in adsorption . . . . .	44
2.2.2. Adsorption thermodynamics . . . . .	45
2.3. Measuring the enthalpy of adsorption . . . . .	49
2.3.1. Isostatic enthalpy of adsorption . . . . .	49
2.3.2. Microcalorimetry . . . . .	50
2.3.3. Experimental apparatus and accuracy . . . . .	52
2.4. Measurements and analysis . . . . .	53
2.4.1. Comparison between enthalpies of adsorption measured through the direct and indirect method . . . . .	53
2.4.2. An example dataset on a reference material . . . . .	54
2.4.3. A study on a novel MOF . . . . .	56
2.5. Conclusion . . . . .	59
Bibliography . . . . .	61
<b>3. Exploring the impact of synthesis and defects on adsorption measurements</b>	<b>64</b>
3.1. Introduction . . . . .	64
3.2. The defective nature of MOFs . . . . .	66
3.2.1. Types of crystal defects and their analogues in MOFs . . . . .	66
3.2.2. Consequences of defects . . . . .	68
3.2.3. Defect engineering of MOFs . . . . .	69
3.2.4. The propensity of UiO-66(Zr) for defect generation . . . . .	69
3.3. Materials and methods . . . . .	71
3.3.1. Materials . . . . .	71
3.3.2. Methods for quantifying defects . . . . .	72
3.4. Results and discussion . . . . .	74
3.4.1. Crystallinity of leached samples . . . . .	74
3.4.2. NMR . . . . .	74
3.4.3. Thermogravimetry results . . . . .	74
3.4.4. Nitrogen sorption at 77K . . . . .	77
3.4.5. Characterisation of trends . . . . .	77
3.4.6. Carbon dioxide isotherms . . . . .	83
3.5. Conclusion . . . . .	84
Bibliography . . . . .	85
<b>4. Exploring the impact of material form on adsorption measurements</b>	<b>90</b>
4.1. Introduction . . . . .	90

## Contents

4.2. Shaping in context . . . . .	91
4.3. Materials, shaping and characterisation methods . . . . .	93
4.3.1. Materials . . . . .	93
4.3.2. Shaping Procedure . . . . .	94
4.3.3. Characterisation of powders and pellets . . . . .	95
4.3.4. Sample activation for adsorption . . . . .	95
4.4. Results and discussion . . . . .	95
4.4.1. Thermal stability . . . . .	95
4.4.2. Adsorption isotherms at 77K and room temperature . . . . .	97
4.4.3. Room temperature gas adsorption and microcalorimetry . . . . .	99
4.4.4. Vapour adsorption . . . . .	105
4.5. Conclusion . . . . .	112
Bibliography . . . . .	113
<b>5. Exploring novel behaviours</b>	<b>115</b>
5.1. Introduction . . . . .	115
5.2. Compliance in porous crystals . . . . .	116
5.2.1. Examining the assumption of an inert adsorbent . . . . .	116
5.2.2. Flexibility in metal organic frameworks . . . . .	117
5.2.3. Describing and inducing MOF compliance . . . . .	119
5.2.4. Consequences and applications of flexible MOFs . . . . .	120
5.2.5. Unique flexible behaviour of DUT-49 . . . . .	121
5.3. Materials and characterisation methods . . . . .	122
5.3.1. Materials . . . . .	122
5.3.2. Characterisation methods . . . . .	123
5.4. Results and discussion . . . . .	126
5.4.1. The structural transition leading to NGA in DUT-49 . . . . .	126
5.4.2. Impact of framework structure on transition mechanics . . . . .	129
5.4.3. An in-depth look at the NGA mechanism . . . . .	136
5.5. Conclusion . . . . .	136
Bibliography . . . . .	137
<b>A. Common characterisation techniques</b>	<b>142</b>
A.1. Thermogravimetry . . . . .	142
A.2. Bulk density determination . . . . .	142
A.3. Skeletal density determination . . . . .	143
A.4. Nitrogen physisorption at 77 K . . . . .	143
A.5. Vapour physisorption at 298 K . . . . .	143
A.6. Gravimetric isotherms . . . . .	144



## Contents

A.7. High throughput isotherm measurement . . . . .	144
A.8. Powder X-ray diffraction . . . . .	144
A.9. Nuclear magnetic resonance . . . . .	144
A.10. Adsorption manometry and calorimetry at 303 K . . . . .	144
Bibliography . . . . .	144
<b>B. Synthesis method of referenced materials</b>	<b>120</b>
B.1. Takeda 5A reference carbon . . . . .	120
B.2. MCM-41 controlled pore glass . . . . .	120
B.3. Zr fumarate MOF . . . . .	120
B.4. UiO-66(Zr) for defect study . . . . .	121
B.5. UiO-66(Zr) for shaping study . . . . .	121
B.6. MIL-100(Fe) for shaping study . . . . .	121
B.7. MIL-127(Fe) for shaping study . . . . .	122
Bibliography . . . . .	122
<b>C. Appendix for chapter 4</b>	<b>123</b>
C.1. Calorimetry dataset UiO-66(Zr) . . . . .	123
C.2. Calorimetry MIL-100(Fe) . . . . .	124
C.3. Calorimetry MIL-127(Fe) . . . . .	127
Bibliography . . . . .	127
<b>D. Calculation of uncertainty in adsorption measurements</b>	<b>129</b>
Bibliography . . . . .	129
<b>D. Appendix for chapter 3</b>	<b>129</b>
D.1. Acid and solvent properties . . . . .	129
D.2. Powder diffraction patterns . . . . .	130
D.3. TGA curves . . . . .	130
D.3.1. DMF leached samples . . . . .	130
D.3.2. Water leached samples . . . . .	131
D.3.3. Methanol leached samples . . . . .	132
D.3.4. DMSO leached samples . . . . .	133
D.3.5. High resolution curves . . . . .	134
D.4. Nitrogen sorption isotherms . . . . .	135
D.4.1. DMF leached samples . . . . .	135
D.4.2. H <sub>2</sub> O leached samples . . . . .	136
D.4.3. MeOH leached samples . . . . .	137
D.4.4. DMSO leached samples . . . . .	138
D.5. Characterisation . . . . .	139

## *Contents*

Bibliography . . . . .	140
<b>E. Appendix for chapter 5</b>	<b>141</b>
Bibliography . . . . .	141

## 5. Exploring novel behaviours

### 5.1. Introduction

Until this chapter, it has been assumed that the porous materials are static when adsorbing a gas. Differences in pore size, crystallinity or structure may exist, but these properties did not change as the host fluid enters the pores. In most cases this is a reasonable assumption. However, it is not universally applicable, as the forces and interactions exerted during adsorption may induce changes in solid itself.

Such effects in classic porous inorganic materials like zeolites, carbons and clays take the form of structural contraction and expansion, swelling or counterion displacement.<sup>(1)</sup> It is only recently that flexibility was discovered in coordination polymers, such as MOFs. A feature which arises from their comparatively weak coordination bonds or pliant organic components, it allows for a systematic deflection of bonds throughout the entire crystal lattice. As such, the term “soft porous crystals” defines porous solids that are both highly ordered and possess the ability to reversibly transform their structure upon external stimuli. Part of the so-called third generation of crystalline porous compounds, they represent some of the latest developments in the field of MOFs.

The unique properties of flexible materials can result in their application in fields such as sensing, micromechanical devices and highly efficient gas storage. It is these perspectives that make their synthesis and design a key research interest. However, their flexible nature introduces new challenges in their characterisation, as factors such as temperature and thermal history<sup>(2)</sup>, crystal size<sup>(3,4)</sup>, external pressure<sup>(5,6)</sup>, structural defects<sup>(7)</sup> and even adsorption kinetics play a role in their compliance. This type of variability goes beyond what has been insofar discussed in this thesis and it is here where a combined characterisation approach becomes essential in understanding the fundamental physics governing flexibility and potential prediction of adsorption behaviour.

### Summary

After a brief introduction of the background of soft porous materials, this chapter will present the characterization of a novel flexible MOF (DUT-49) and its analogues. This material un-

dergoes a sudden collapse of its pore network into a closed form state upon adsorption, resulting in the expulsion of gas from its pores. This phenomena was coined “negative gas adsorption” (NGA). The text will focus on characterisation through calorimetric methods performed by Paul Iacomi, together with references of results obtained by collaborating groups included in order obtain a complete story of the underlying mechanism behind NGA.

### Contribution

The synthesis of all MOFs was performed by Simon Krause (TU Dresden), together with their initial characterization through nitrogen adsorption at 77 K. Ambient and low temperature calorimetry was carried out by Paul Iacomi. Computer simulations of adsorption isotherms are the result of work from Jack Evans and Prof. FX Coudert. Mechanical compression experiments were performed in the group of Prof. Guillaume Maurin in Montpellier. Prof. Philip Llewellyn and Prof. Stefan Kaskel were instrumental in the analysis of the results obtained.

## 5.2. Compliance in porous crystals

### 5.2.1. Examining the assumption of an inert adsorbent

Adsorption induced changes in porous media have been known to occur for over 90 years<sup>(8)</sup>, with both clays, coals and polymers undergoing swelling during gas or vapour uptake.<sup>(9)</sup> However, the effect upon the macroscopic properties of the material is often negligibly small and of little consequence to industrial adsorption processes. Studies of this aspect of porous adsorbents have therefore been scarce in the large part of the 20<sup>th</sup> century, likewise influenced by lack of sufficiently accurate methods for characterising and modelling such occurrences.

In recent years, the advent of reference materials, highly sensitive methods such as synchrotron-grade light sources and *in silico* computational techniques such as DFT has put at our disposal the tools required to study these transformations. Together with the discovery of their role in natural and industrial processes e.g. the swelling of shale during natural gas extraction, maturation of concrete and the perspectives afforded by novel porous materials, these factors have generated much scientific interest in material compliance. For example, the attractive option of combined carbon capture and methane recovery implemented through pumping of carbon dioxide into reservoirs is prohibited by swelling-induced loss of porosity and well blocking.<sup>(9)</sup>

In-depth studies<sup>(10)</sup> have revealed that most porous materials posses some small degree

of compliance, with *in-situ* dilatometry going so far as to obtain pore size distributions from accurate volume changes.<sup>(11)</sup> Most flexible processes can be likened to continuous order processes. It is, however, the discovery of large scale flexibility in MOFs such as MIL-53 and linker-controlled gate opening like in ZIF-8, where the transformation between the different framework states occurs suddenly at precise points in the loading curve, which has shown that compliance may also take the form of a first-order transition. Such types of transformations are desirable<sup>(12)</sup> due to their highly specific response. The possible dependence of flexibility on other stimuli, such as light, mechanical pressure, temperature, magnetic fields may allow for precise tuning of structural changes. As such, it is reasonable to state that the mobility of the solid phase can no longer be ignored.

### 5.2.2. Flexibility in metal organic frameworks

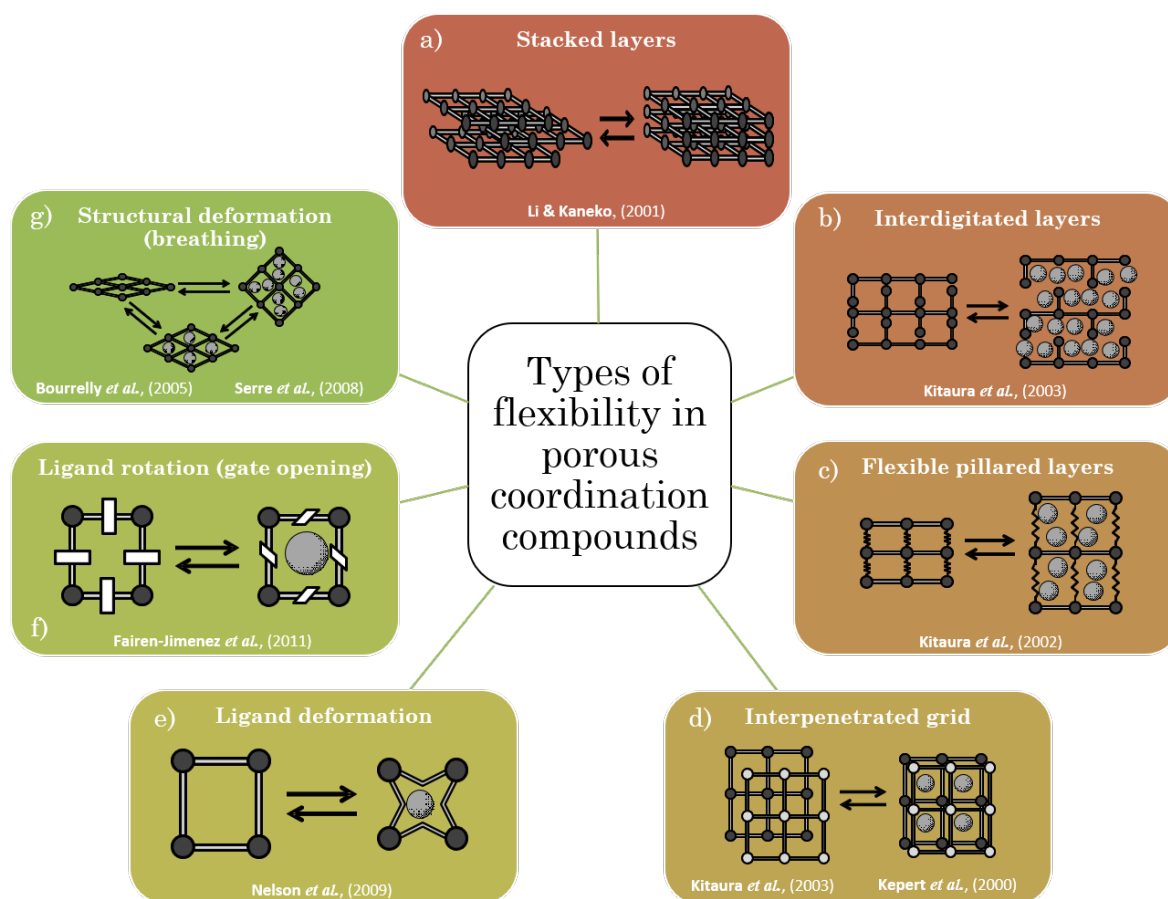
Since the highlight of compliance in porous coordination polymers in the report of Kitagawa et al.<sup>(12)</sup>, much progress has been made in the synthesis and understanding of this phenomenon. An exhaustive review of MOF flexibility is outside the scope of this thesis, with the field progressing rapidly enough to generate a wealth of critical literature.<sup>(13–19)</sup> Some of the known types of structural flexibility encountered in MOFs will be briefly discussed, with a summary available in Figure 5.1.

Since MOFs, like clays and graphite, can form discrete two-dimensional sheets, bound together by weak Van-der-Waals,  $\pi - \pi$  interactions or hydrogen bonds, adsorbed molecules may force these layers apart by intercalation. The concept is taken further in the pillared layer approach, where the sheets are connected by tertiary linkers instead of weak attractions. With the judicious choice of linker they can act as springs, allowing pore expansion while maintaining structural integrity.

As briefly mentioned in chapter 3, a large void space in the unit cells allows secondary networks to grow throughout the MOF, effectively creating an intercalated structure.<sup>(21,23)</sup> These secondary grids are independent of the primary framework and are displaced upon guest adsorption.<sup>(28)</sup> This internal translation may also be associated with a tilting of the linker<sup>(29)</sup>, combining intercalation with structural-deformation type flexibility.

The origin of flexibility may be purely due to the linker itself. Organic bonds are inherently labile, as seen in polymer chains, unsaturated connections in the linker may bend if the strain on the organic strut overcomes its tensile strength. Increasing the linker length often induces this type of flexibility, for example in the IRMOF isorecticular series of materials.<sup>(24)</sup> Even an unsaturated bond may be induced by a photon with a suitable energy to undergo an analogue of a *cis-trans* transition. The deformation may also lead to expansion and therefore of framework swelling, as encountered in MIL-88 and its derivatives.<sup>(30)</sup>

## 5. Exploring novel behaviours



**Figure 5.1.:** A (non-exhaustive) visual summary of the types of flexibility documented in MOFs, as detailed in (a) Li and Kaneko<sup>(20)</sup> (b) Kitaura et al.<sup>(21)</sup> (c) Kitaura et al.<sup>(22)</sup> (d) Kitaura et al.<sup>(21)</sup>, Kepert et al.<sup>(23)</sup> (e) Nelson et al.<sup>(24)</sup> (f) Fairen-Jimenez et al.<sup>(25)</sup> (g) Bourrelly et al.<sup>(26)</sup>, Serre et al.<sup>(27)</sup>

MOFs can also have structural flexibility which does not require any volume changes in the unit cell. The rotation of linkers can act as gating for different guests, allowing entry of probes larger than the window size would suggest or preferential adsorption of a gas which has the right property to act as a “key” from a mixture.<sup>(31)</sup> The former effect is common in zeolitic imidazole frameworks (ZIFs).<sup>(25)</sup>

The discovery of the so-called “breathing” type of structural deformation<sup>(26,27,32)</sup> in the MIL-53 family of materials has revealed step-like transformations in its unit cell size and metastable intermediaries with an open pore (**op**), closed pore (**cp**) and narrow/intermediate states (**np/ip**). No other family of flexible MOFs has, to date, generated more scientific interest. This is likely due to the relative stability of the material, combined with its ability to undergo massive and reversible structural deflections, while retaining its crystallinity. The relatively simple structure and large capability for functionalisation, either through ligand modification or exchange of the metal node (with variants of MIL-53 synthesised for Cr, Fe, Al, Sc, Ga or In), allowed for its use as an archetypal material for the study of flexible be-

haviour. More recently, similar materials, like DUT-8(M) (M=Ni, Co, Cu, Zn) which allow the the impact of the metal<sup>(33)</sup> on compliance to be evidenced have emerged.

### 5.2.3. Describing and inducing MOF compliance

The mechanistic phenomena during adsorption can be seen as an overlap<sup>(34)</sup> of several competing effects: a sub-monolayer contraction<sup>(35)</sup> resulting from micropore bridging or surface stresses, followed by a monotonic expansion with the gradual decrease of the solid-fluid interface energy also known as the Bangham effect.<sup>(36)</sup> Such behaviour is highly dependent of pore size, geometry and anisotropy, with condensation in macropores a further complex source of strain.<sup>(37–39)</sup> The degree of adsorption induced changes in a framework is generally a function of its porosity, with very high surface area materials such as aerogels capable of undergoing up to 30% deformation.<sup>(40)</sup> In MOFs, the adsorption stresses are no different than in other materials. However, the ability of the porous network to undergo displacements is much higher, due to its low rigidity, in between that of “hard” adsorbents such as zeolites/silica and purely organic polymers (although porous covalent frameworks can also achieve self-support and porosity).

Finding a suitable model that would predict both the adsorption induced stress and the resulting structural changes from strain has so far remained a challenge. A thermodynamic-based method which has been successfully applied to breathing MOFs is that of Neimark et al.<sup>(41)</sup>. This model assumes that the deformation strain is fully determined due to surface stress, calculated from the grand thermodynamical of a rigid analogue of the pore. It has been used to explain the existence domains of MIL-53(Al)<sup>(42)</sup>, in conjunction with an osmotic thermodynamic description of the framework itself.<sup>(43)</sup> For mesoporous materials, the stress-strain model has been extended by Gor and Neimark<sup>(34)</sup> through the Derjaguin–Broekhoff–de Boer (DBdB) theory<sup>(44)</sup> and applied to predict the resulting strain in mesoporous silica. Nevertheless a complete theory of adsorption-deformation which can fully predict the changes in the measured enthalpy of adsorption and the mechanistic behaviour of MOFs has remained elusive.

The most promising characteristics of flexible MOFs are the ability to control the compliance through external means which are detached from guest loading, which would dramatically expand their potential applications. Pure mechanical pressure on a flexible material is often enough to induce transitions. First observed on ZIFs, through pressure induced phase change<sup>(45,46)</sup> and latter applied to breathing MOFs using mercury porosimetry<sup>(47,48)</sup>, it shows a direct relationship between the bulk modulus of a MOF and its flexible behaviour. Entropic control through temperature-induced switching has been shown to be possible in MIL-53 by Liu et al.<sup>(2)</sup>, explained as a change in the range of metastability of its pore forms.<sup>(42)</sup> More precise external control may be possible if molecules which have the ability

to switch their state when exposed to suitable wavelengths are used as linkers. In this case light irradiation may be used to force the transition.<sup>(49)</sup> Magnetic field dependent switching can also be theorised, although has not been so far encountered. One of the least understood factors that changes the flexible behaviour of porous crystals is the effect of particle size. It is clear that the thermodynamical potential of the crystal surface has a profound influence on its compliance, as shown on the large shift of the gate-opening pressure of ZIF-8.<sup>(3)</sup> However, a rigorous model of the contribution of the surface on breathing has yet to be developed in our knowledge. Finally, the presence of structural defects likely impacts the framework flexibility, as highlighted by Bennett et al.<sup>(7)</sup> in a recent article, although currently few studies have focused on this subject.

### 5.2.4. Consequences and applications of flexible MOFs

The study of flexible MOFs is motivated from both a desire for fundamental understanding of compliance and from the potential applications of such systems. The use of soft porous crystals in sensing and gas storage and separation is evident, although applications in catalysis, electrochemistry and drug delivery have also been alluded to by recent studies.

The usefulness of adsorption induced flexibility for sensors or actuators has been recognised, initially by nature itself, with humidity induced swelling acting to open pine cones.<sup>(50)</sup> More recently, similar sensing devices based on adsorption strain in mesoporous silica have been developed such as a flexing silica-polymer membrane<sup>(51)</sup> or deformation of a nano sized cantilever<sup>(52)</sup> which show promise for use in micromechanical systems.

From a gas storage and separation point of view, changes in the adsorbent structure may yield crucial process improvements. Pressure swing adsorption (PSA) is heavily dependent on the working capacity of the adsorbent used, or the difference between loading at the operation pressure and at the regeneration pressure. In this case, an S-shaped isotherm, with the vertical part of the slope in the aforementioned pressure range would lead to high process efficiency gains by eliminating material “dead volume adsorbed”.<sup>(13)</sup> In a temperature swing process (TSA), where the regeneration is performed through heating of the adsorbent bed, the key parameter is the integral enthalpy of adsorption, a measure of the energy requirements for the process. As a part of the chemical potential of the adsorbed phase is used by the mechanical contraction of the material, flexible adsorbents have the potential of intrinsic thermal management, reducing the energy cost.<sup>(53)</sup> Both effects are equally applicable to the storage of pure gasses, increasing the storage capacity and minimizing the energetic requirement of recovery. Entrapment of guest molecules inside a gated pore might lend itself to temperature controlled storage and release of gasses<sup>(54)</sup>, or “sealing” of a target gas inside the structure once adsorption has taken place. It is also possible that by using external mechanical pressure to control flexibility, the adsorption behaviour of porous



materials may be tuned, as suggested by the work of Chanut<sup>(6)</sup> on MIL-53.

Catalytic applications of flexible MOFs could be envisaged where the switching behaviour can bring into contact active sites or hold reactants in place until complete reaction has taken place. A recent study by Souto et al.<sup>(55)</sup>, has shown that the redox potential of the sulphur bond in a tetrathiafulvalene breathing MOF is dependent on its dihedral angle in different pore states. This raises the possibility of tunability of the oxidation potential of flexible framework. Finally flexible MOFs constructed of biocompatible materials could be used as drug delivery methods<sup>(56,57)</sup> if release of the encapsulated molecule is triggered through a structural transition.

### 5.2.5. Unique flexible behaviour of DUT-49

It is clear that one of the most desirable kinds of flexibility is one that can be likened to a Heaviside step function, with switching between two states or phases. However, not many MOFs synthesised to date follow this type of behaviour. It is why the surprising compliance of DUT-49, a highly porous MOF constructed with a super-molecular approach, has generated interest in the MOF community.

In the initial paper of Stoeck et al.<sup>(58)</sup>, the synthesis of DUT-49 through a super-molecular approach is described, with the goal of generating a highly porous material. The MOF is built through the secondary building unit or SBU approach, where the crystallographic vertices of the structure are metal organic polyhedra (MOP), in this case 12-connected cuboctahedra based on copper paddlewheels, which are then connected by a tetratopic carboxylate linker. The resulting MOF forms a face centered cubic (**fcu**) net if the MOP are considered as nodes and a trimodal pore size distribution: the 12 Å MOP, a 18 Å tetrahedron and a very large 26 Å octahedron. The material has a high nitrogen accessible surface area (of more than 5000 m<sup>2</sup>/g) and accessible volume (84.7%).

In the original study, the MOF did not show any flexible behaviour. However, it was later found by Krause et al.<sup>(59)</sup> that when adsorbing CH<sub>4</sub> at 111 K, a sharp step occurs in the isotherm, corresponding to an **op/cp** transition. More interestingly, the step is accompanied by an expulsion of the adsorbed gas from the interior of the pores, increasing the pressure in the experiment cell. This type of pressure-amplifying transition has been coined negative gas adsorption (NGA) and was found to occur with other adsorbates at different temperatures such as C<sub>4</sub>H<sub>10</sub> at 303 K or Xe at 195 K, which allowed study of the transition at ambient temperature and through <sup>129</sup>Xe NMR spectroscopy.<sup>(60)</sup>

The origin of this phenomenon has been elucidated by Evans et al.<sup>(61)</sup> where it has been shown to emerge due to a buckling of the central strut of the tetratopic linker under compressive stress induced by adsorption, similar to the failure of a metal column under critical

load. The **op** and **cp** phase stability depends on the adsorbate loading of the material, with the **op** form being energetically favoured at zero and high loadings. At intermediate pore filling, the **cp** state is stabilized by the fluid molecules and becomes energetically favoured. At this point, the **op** phase is metastable and can contract if the energy barrier between the two states is overcome. As the transition from the **cp** to the **op** state requires an activation energy, re-opening of the structure is only possible through complete structure loading. If the system is in its **cp** state during adsorbate removal, the structure undergoes complete structural collapse.

However, questions still remain about the driving forces behind the transition itself such as the contribution of guest-host interactions, as well as the temperature range and adsorbates where it is possible. The rational design of such materials is also put into question, where framework parameters such as linker length, functionalisation and composition may be used to tune the pressure and extent of NGA. It is here where the adsorption methodology introduced in chapter 1 combined with *in-situ* calorimetry as presented in chapter 2 can be used to shed light on the energetic background of NGA in DUT-49.

### 5.3. Materials and characterisation methods

#### 5.3.1. Materials

Several DUT materials have been synthesised in order to study the effect of different parameters on the switching behaviour. From the point of view of the criterion of interest, the materials can be divided into the following categories:

- Series dedicated to studying the influence of isorecticular design through variation of linker length in the order of theoretical increasing porosity: DUT-48, DUT-46, DUT-49, DUT-50, DUT-151/DUT-152. These materials are designed with a linker of increasing size by using differently structured phenyl rings. A corresponding increase in porosity is expected, however, starting from a 4-linear phenyl chain (DUT-151), the internal voids are large enough to allow for a secondary interpenetrated network to develop. An attempt to prevent this by grafting bulky naphthalene rings was made in the synthesis of DUT-152, but the resulting structure was still found to be interpenetrated.
- Series assessing the impact of steric hindrance of the central linker bond on NGA, in the order of connectivity: DUT-49, DUT-149, DUT-148, DUT-147. The rationale behind this approach is to improve the tensile strength of the strut by the addition of sterically hindering side connections.
- Series investigating the effect of heterocycles on compliant behaviour, using thiophene as replacement for the benzene rings, in the order of increasing linker size: DUT-170,

## 5. Exploring novel behaviours

DUT-171, DUT-172, DUT-173. If interactions with the framework plays a role in NGA, the addition of potentially stronger host-guest sites.

- Series aiming to possess a progressively more labile central strut through the use of different degrees of saturation, in order of central bond hybridization: DUT-160, DUT-161, DUT-163. It was found that the removal of solvent from DUT-162 could not be performed without structure collapse. The softness of the saturated backbone lends itself to an unstable **op** state.
- Series of increasing crystallite size to study the effect of the crystal surface to volume ratio on NGA. Different sizes of DUT-49 were synthesised either through the addition of an acid modulator for obtaining large crystals or through the addition of a base to inhibit crystal growth. A series of 4 DUT-49 was received, of 800 nm, 1  $\mu\text{m}$ , 4  $\mu\text{m}$  and 10  $\mu\text{m}$  average size respectively.

The material name, together with the central part of the linker, which was modified to change the flexible behaviour of the framework, is presented in Table 5.1.

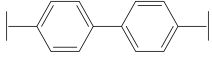
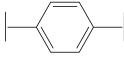
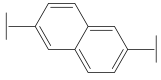
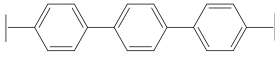
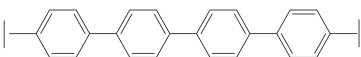
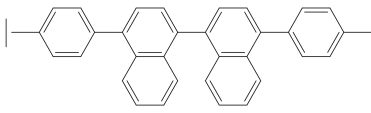
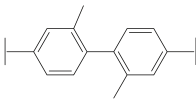
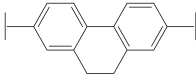
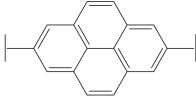
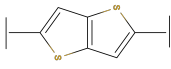
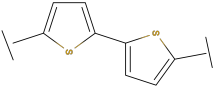
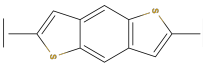
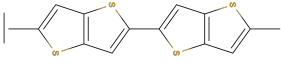

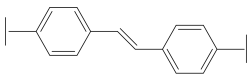
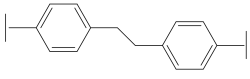
### 5.3.2. Characterisation methods

In order to examine the energetic components of both adsorption and NGA, the combined manometry and calorimetry methodology first presented in chapter 2 was used. Ambient temperature calorimetry was conducted at 303 K with probes such as butane, propane and propylene using the step-by-step gas introduction method. The exact procedure for such an experiment can be found in section A.10 of Appendix A.

For low temperatures (77 K), a high resolution continuous introduction method was employed, together with a home-made calorimetric system first described in the work of Rouquerol et al.<sup>(62)</sup>. To summarize, the adsorbate is placed in a J-shaped custom designed glass cell which is then sealed with an oxyacetylene torch prior to evacuation and sample activation. Borosilicate glass is selected as the material of choice to prevent any thermal expansion induced leaks. The cell is then introduced into a  $\text{LN}_2$ -filled dewar, through the bottom of the differential calorimeter. Good thermal equilibrium between the cell and surrounding thermopile is ensured using by using a helium blanket in the calorimetric enclosure, kept under positive pressure through a continuous low flow. The connection to the gas dosing system is made through a Swagelock VCR  $1/4''$  stainless steel connection. High leak resistance and gas purity is assured by the single use copper joint metal-to-metal interlock. Pressure is measured through the use of a double gauge assembly, a sensitive low pressure gauge (up to 2 kPa) and an ambient pressure gauge (up to 120 kPa). A sonic nozzle is used to control the flow of adsorbate into the reference volume and the cell. A separate calibration step is performed at the start of each experiment to determine the adsorbate flowrate

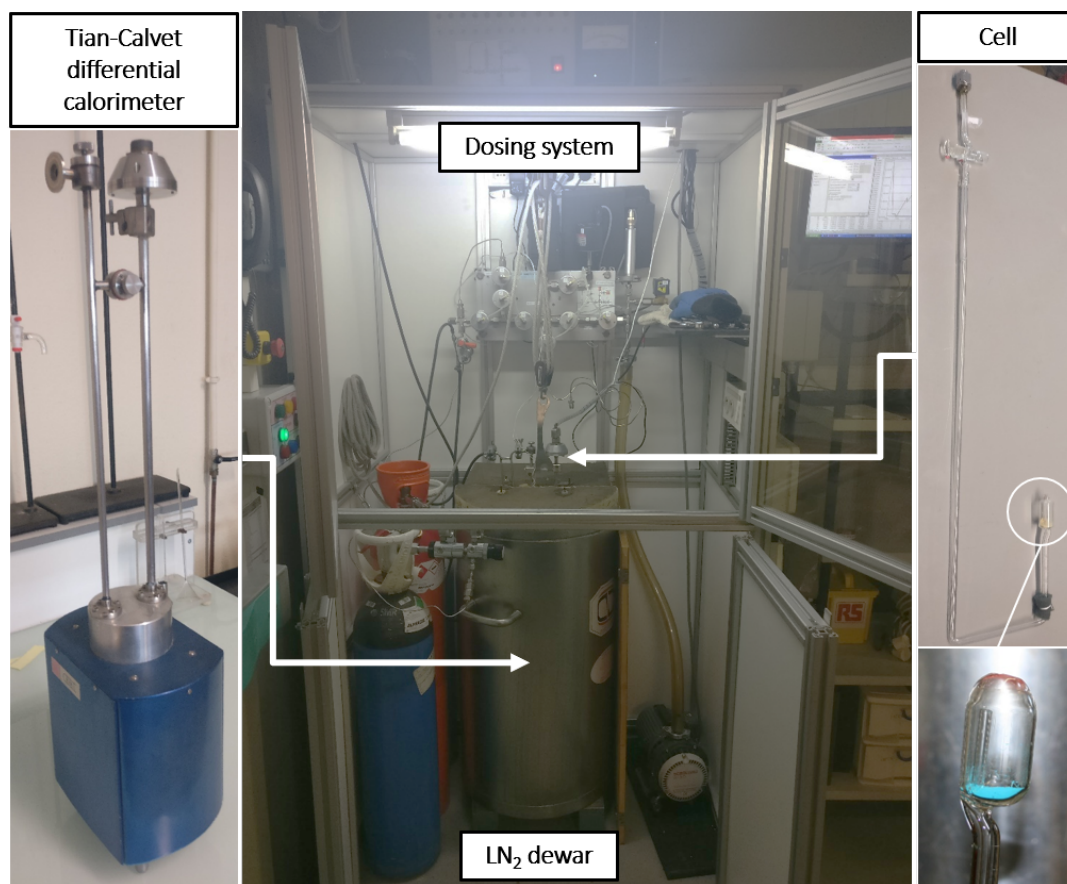
## 5. Exploring novel behaviours

**Table 5.1.:** Flexible materials analogous to DUT-49

Name	Linker center	Study	Observations
DUT-49		Original material	Multiple crystal sizes <ul style="list-style-type: none"> <li>• DUT-49(o)-0.8 <math>\mu\text{m}</math></li> <li>• DUT-49(s)-1.0 <math>\mu\text{m}</math></li> <li>• DUT-49(m)-4.0 <math>\mu\text{m}</math></li> <li>• DUT-49(l)-10.0 <math>\mu\text{m}</math></li> </ul>
DUT-48		Linker size	—
DUT-46		Linker size	—
DUT-50		Linker size	—
DUT-151		Linker size	Interpenetrated
DUT-152		Linker size	Interpenetrated
DUT-149		Functionalization	—
DUT-148		Functionalization	—
DUT-147		Functionalization	—
DUT-170		Heterocycle	—
DUT-171		Heterocycle	—
DUT-172		Heterocycle	Not measured
DUT-173		Heterocycle	Not measured
DUT-160		Strut saturation	—
DUT-161		Strut saturation	Not measured
DUT-162		Strut saturation	No stable <b>op</b> state

## 5. Exploring novel behaviours

and the dead volume before the entrance to the cell. An experiment takes between 1–4 days depending on the flowrate used. A picture of the different components of the setup can be seen in Figure 5.2.



**Figure 5.2.:** The low temperature calorimetry setup

Extreme care has to be taken during sample preparation, as all materials studied are sensitive to heat and water vapour, which quickly destroy the Cu paddlewheel. To prevent any decomposition, the samples were stored under an inert argon atmosphere in a glovebox. The loading of ambient temperature cells was performed inside the glovebox while filling and sealing of low temperature glass cells was done in an argon flow. After sample cell preparation, the materials are activated under dynamic vacuum at 120 °C.

It is worth noting that if the sample undergoes an **op/cp** phase transition during the experiment and cannot be reopened with the application of high pressure, as is the case for butane at 303 K, the material cannot be reused since any attempt to activate it under vacuum leads to structural breakdown of the unstable **cp** phase. Since a limited amount of sample is available, this played a large role in data acquisition, with several isotherms only recorded once.

## 5.4. Results and discussion

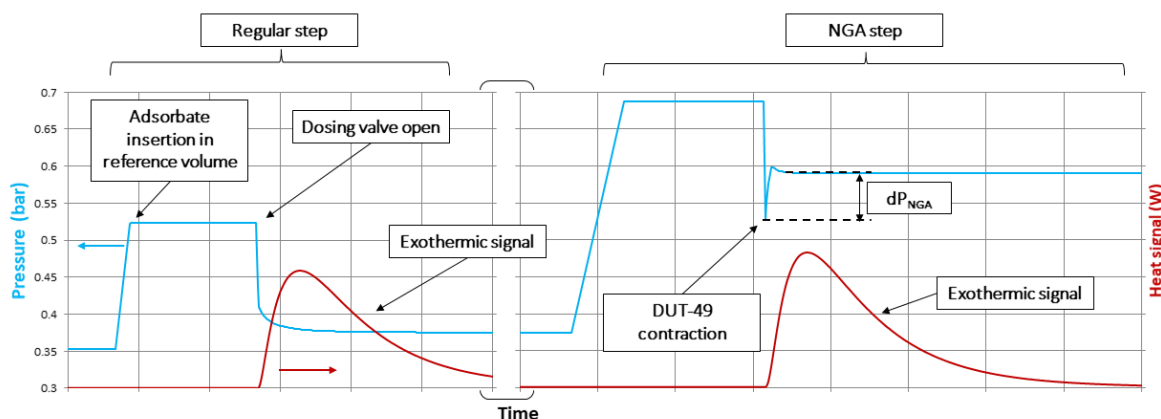
The first part of this section will present the characteristics of the NGA step in DUT-49 as recorded by ambient calorimetry, and what a cursory examination of the isotherm and enthalpy curves at 303 K can reveal about the energetics of the system and the stability of the two phases.

The following subsection contains the results of the studies on DUT-49 analogues, highlighting the effects that linker elongation and functionalization have on the adsorption behaviour and NGA extent at ambient temperature.

Finally, an in-depth study of the DUT-49 NGA mechanism is performed, employing a variety of gas probes ( $\text{N}_2$ , Ar,  $\text{O}_2$ , CO) at low temperature. The time-resolved data obtained through continuous adsorbate introduction sheds light on the influence of the host-guest and guest-guest interactions on transition mechanics, the energetic barrier of the transition state and on system kinetics. A comparison with non-flexible analogues allows an assessment of the role of the pore filling mechanism on the structural transition to be made.

### 5.4.1. The structural transition leading to NGA in DUT-49

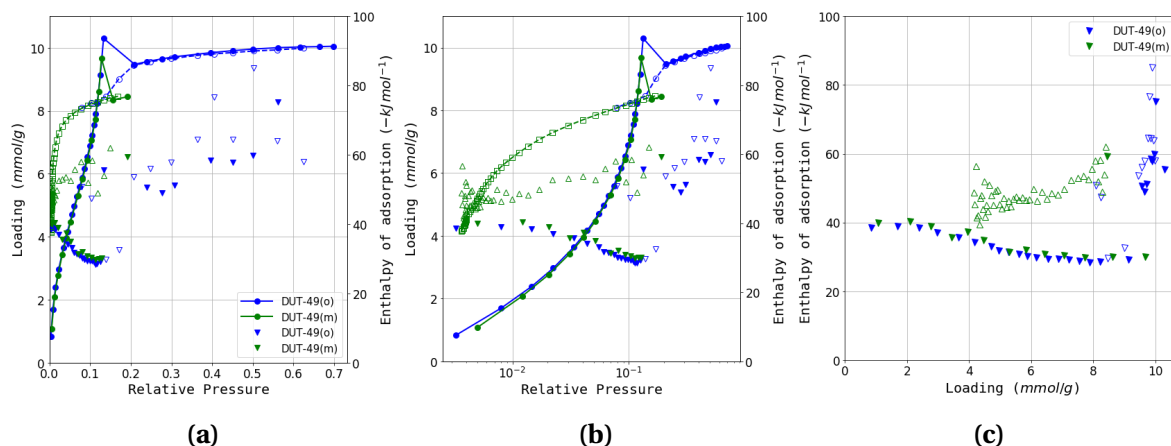
In the time-resolved pressure and calorimetry signal recorded when performing butane adsorption at 303 K, the NGA step is clearly visible as the pressure in the cell suddenly increases after a dosing point. An example can be seen in Figure 5.3, next to a regular dosing step. A short time after the adsorbate is introduced in the measurement cell, the material contracts. The calorimeter signal is positive, therefore the overall process is still exothermic — even though desorption and structural transition, both endothermic processes, are taking place.



**Figure 5.3.:** The pressure and calorimeter signal from butane adsorption on DUT-49, highlighting a typical step (left) and the observed NGA step (right)

## 5. Exploring novel behaviours

The signals are then processed to yield the combined isotherm and differential heat of adsorption. Figure 5.4 shows two isotherms recorded on different DUT-49 samples. Several observations can be made. First, a clear transition takes place around  $0.15 p/p_0$ . This corresponds to the **op**/**cp** transition which *decreases* the amount adsorbed per gram of material. After NGA, the material is in its **cp** form, where it remains throughout the remainder of the measurement. Unlike in the methane experiments performed at 111 K, the structure does not re-open. A secondary transition to the **op** form is expected at higher pressures, close to the saturation pressure of the adsorbate. However, this pressure range could not be reached within the experimental conditions.



**Figure 5.4.:** Butane adsorption experiments on two samples of DUT-49, DUT-49(o) and DUT-49(m) shown as (a) regular isotherms (b) logarithmic isotherms and (c) enthalpy as a function of pressure.

Due to the steep knee in the adsorption/desorption branch of the **cp** form, a complete desorption branch cannot be obtained, with the minimum attained loading of 4 mmol. As such, framework collapse is not seen in the experiments. Another shortcoming is that the isotherm and energy landscape of the **op** form in its metastable region is inaccessible, since by definition the material will undergo a transition in this pressure range.

Another key feature visible in the two recorded isotherms is that, while adsorption on the open pore form fully overlaps between the two experiments, both the location and extent of NGA differ slightly. In the DUT-49(o) isotherm, a smaller NGA step occurs, with the resulting structural contraction apparently unable to achieve a complete closing of the pores. Upon desorption, a secondary step occurs in the same  $0.15 - 0.2$  pressure range, after which the material is fully in its **cp** state, as evidenced by the overlap with the DUT-49(m) isotherm. The reason behind the dissimilar behaviour is the contribution of crystal size to the energy barrier of transition. A thorough analysis can be found in the paper published by Krause et al.<sup>(4)</sup> where it is shown that a high surface to volume ratio has a negative impact on NGA, with smaller crystallites unable to achieve a complete contraction, instead accessing an inter-mediated or **ip**, with the “*a*” lattice parameter 5–7% smaller than the **op** phase rather than

24% in the **cp** phase.

The enthalpy curves in Figure 5.4c, paint a picture of the energetic landscape of both phases. First it should be noted that the differential enthalpy of the NGA step itself does not appear on the graph as it is a negative value. This is not because the transition step is endothermic, as proven in Figure 5.3. However, as the net change in adsorbed amount between the two points where the transition occurs is negative, the calculated enthalpy *per mol of gas adsorbed* takes the same sign.

In the adsorption branch, the initial enthalpy of adsorption can be observed to be around  $38 \text{ kJ mol}^{-1}$  to  $40 \text{ kJ mol}^{-1}$ . This value is relatively low for a copper-based MOF<sup>(63)</sup> and suggest that the interaction of the pore wall with the adsorbate is relatively low. After  $2 \text{ mmol g}^{-1}$ , the enthalpy curve slopes downwards until a local minima around  $30 \text{ kJ mol}^{-1}$  before NGA. This is the multilayer adsorption region, where the field gradient of the pore wall decreases and guest-guest interactions dominate. The enthalpy calculated for the desorption curve is essentially the differential enthalpy of adsorption on the **cp** form. A large difference, in the range of  $10 \text{ kJ mol}^{-1}$  to  $20 \text{ kJ mol}^{-1}$ , exists between the enthalpy of adsorption in the two states. This can be attributed to the microporous nature of the **cp** form, with the smaller pore walls increasing the interaction of the framework backbone with an adsorbate molecule. The energy required to drive the transition and generate the observed thermal effect can be accounted for by the increased total interactions of remaining adsorbed molecules with the **cp** state of the framework. A more in-depth analysis of the NGA energetics will be presented in subsection 5.4.3.

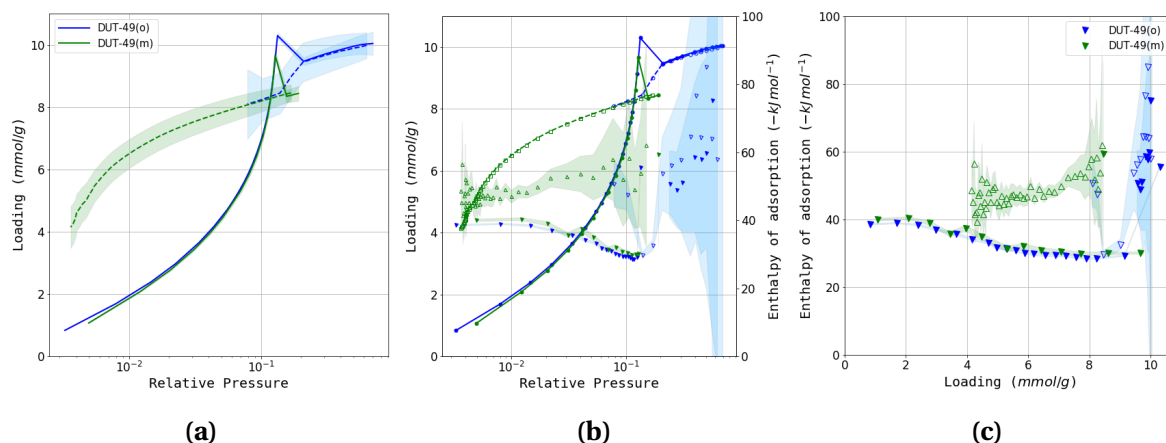
### A brief analysis of measurement uncertainty

In order to assess whether results obtained through calorimetry are within acceptable accuracy, uncertainty calculations have been carried out. The method used here is laid out by the International Organisation for Standardisation (ISO) in the Guide to the expression of Uncertainty in Measurements (GUM). The method is fully detailed in Appendix D, and consists of an identification of all variables used in the calculation of the final result, and estimation of the uncertainty in the final value as a function of the uncertainty in each such variable. The result is multiplied by a factor of confidence, which has been chosen as 95% in the figures presented in Figure 5.5.

The use of the manometric method for isotherm measurement entails a cumulative error in the pressure measurement that leads to an increase in uncertainty with each measured point. It can be seen in Figure 5.5a that in spite of the margin of error, there is perfect overlap between the two measured isotherms in the adsorption branch and in the desorption branch. It is reasonable to assume that the error is therefore much smaller than the calculation would suggest.



## 5. Exploring novel behaviours



**Figure 5.5.:** Estimated errors at a 95% confidence range for (a) loading as a function of pressure, (b) differential enthalpy as a function of pressure (c) differential enthalpy as a function of loading.

The uncertainty in the differential enthalpy of adsorption (Figure 5.5b) is a function of  $\Delta n$ , the amount adsorbed in each step, as well as pressure, with the same cumulative error applicable. The former variable accounts for the large uncertainty in flat sections of the isotherm where almost no adsorption takes place, while the latter results in the spread seen at the end of the desorption curves. However, when observing  $\Delta_{ads} \hat{h}$  as a function of loading in Figure 5.5c, the uncertainty is confined to high values on the x axis, with a clear separation of isotherm branches.

As the display of uncertainty ranges clutter the isotherm graphs and makes it hard to distinguish features, the remainder of this chapter will only display them if the error range is significant.

### 5.4.2. Impact of framework structure on transition mechanics

While the discovery of the NGA transition in DUT-49 was a result of serendipity, it opens the door to a rational design approach to modify the extent and the location of the phenomenon. In principle, there are several avenues that could be taken in order to tune the contraction mechanics.

- Changing the range of metastability of the open pore state.
- Decreasing the porosity of the closed pore state.
- Increasing the capacity of the open pore form.

These factors are bound to be tightly interlinked, with a slight alteration in one possibly leading a shift in all. For example, the addition of a stabilizing group which would increase the tensile strength of the linker is also likely to decrease the porosity of the entire system.

## 5. Exploring novel behaviours

There are a range of physicochemical modifications available to tune the properties of the framework, many already employed in the MIL-53 and MIL-47 family of flexible MOFs. Through functionalisation or modification of the linker, the strength of the guest-guest and guest-host interactions is affected, as evidenced by the different gate opening behaviour with nitrogen and water on several functionalised versions on MIL-53.<sup>(64)</sup> In the case of DUT-49, moieties grafted to the central strut or changes in the linker backbone are also likely to affect its buckling behaviour. The use of a different metal as the node, has succeeded in changing the mechanical response of MIL-53.<sup>(65)</sup> This approach is likely have less impact on DUT-49, as the mechanism of contraction is due to linker flexibility. A common rational design methodology is the so-called isorecticular design, where topologically isomorphic MOFs are synthesised through progressive elongation of the linker. Another path to controlling flexibility is manipulation of crystal size, as it has already been shown by Krause et al.<sup>(4)</sup>. Finally, structural defects, of which a description was given in chapter 3, are another degree of freedom to consider for NGA tunability. Approaches such as mixed linkers synthesis and vacancy defects may allow for fine-grain influence of framework stiffness.

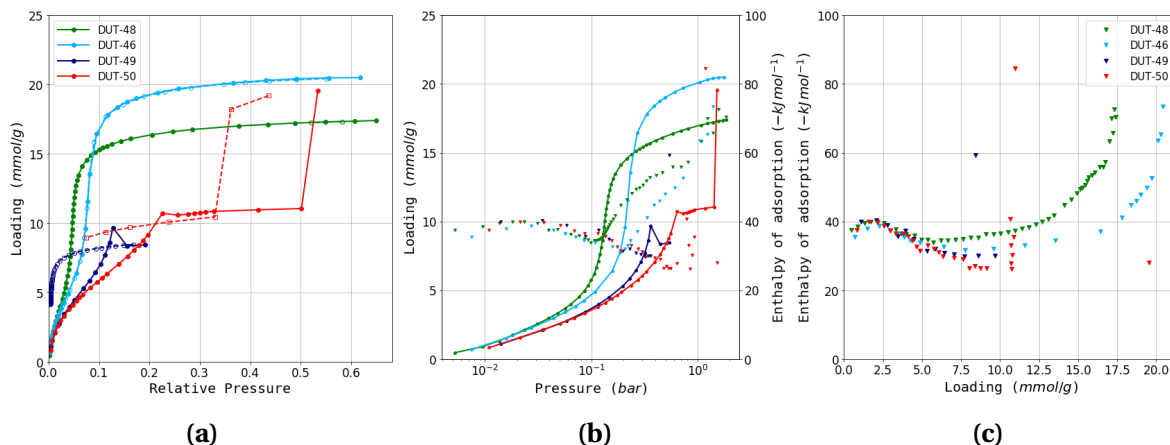
### Behaviour of isorecticular materials

The series of materials DUT-48, DUT-46, DUT-49, DUT-50 and DUT-151/DUT-152 was synthesised with the aim of studying the effect of linker elongation on the NGA step. It was found that the tetra-phenyl chain in DUT-151 increased the pore size to the threshold where a secondary can form in the intracrystal voids, resulting in two identical interpenetrated nets. An attempt to introduce a bulky side-functionalisation in DUT-152 resulted in a similarly interpenetrated material. Figure 5.6 shows the butane adsorption dataset recorded on the non-interpenetrated versions.

Indeed, the results follow a predictable trend. First, it is worth noting that, as seen in Figure 5.6a, only DUT-49 and DUT-50 undergo an **op/cp** transition. This confirms that a shorter linker imparts the resulting MOF with a more stable backbone, raising the strain required in order to collapse the framework. The desorption branch of the non-flexible materials completely overlaps the adsorption branch in both isotherm and enthalpy, further confirming the small error in measurement (available in Figure E.1a). With an increase of linker size, a larger pore volume and consequently a higher amount of butane can be adsorbed in the open pore form. The increase in pore size is also responsible for a shift in the pressure of condensation, or pore filling step.

In DUT-50, the structure is seen to re-open around  $0.5 p/p_0$ , although the pressure is not high enough to completely transition to the **op** form. The collapse to the closed phase in the desorption branch achieves a lower plateau than in the adsorption branch, suggesting an incomplete **op/cp** transition as seen in one of the isotherms on DUT-49 in the previous

## 5. Exploring novel behaviours



**Figure 5.6.:** (a) Experimental adsorption isotherms for DUT-48, DUT-46, DUT-49 and DUT-50. Enthalpy points are omitted for clarity. (b) A logarithmic plot of isotherms and enthalpy curves, to highlight the low pressure region. (c) Differential enthalpy of adsorption as a function of loading.

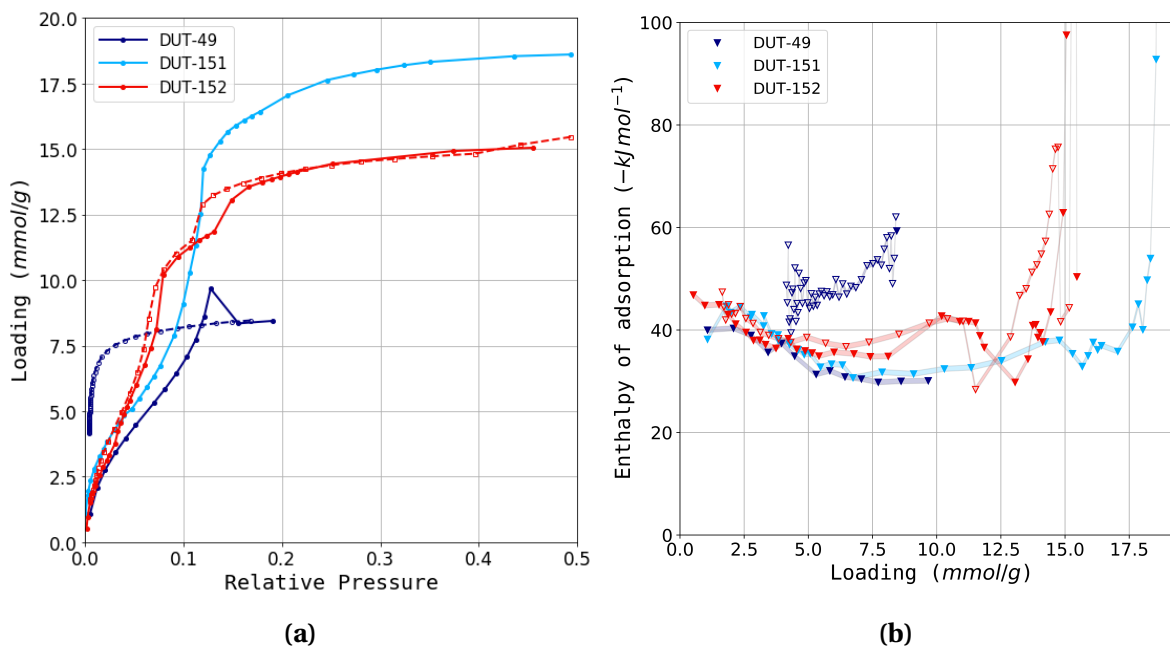
section.

One surprising finding is that the enthalpy curves (Figure 5.6c) present a near identical behaviour and differential enthalpy of adsorption in the low pressure region, characterized by a slight increase up to 40 kJ mol<sup>-1</sup> followed by a drop-off. The adsorption mechanism and surface characteristics are therefore *common* to all four materials. The shift of the enthalpies of adsorption to lower values at higher loadings from DUT-46 to 50 is expected, with the increase in pore size leading to a progressive decrease of the contribution of dispersion interactions with the guest, which could also be referred to as a confinement effect. The steep uptake in the isotherm is indicative of a cooperative adsorption mechanism similar to a fluid condensation, accompanied by an increase in the contribution of guest-guest interactions to  $\Delta_{ads}h$ .

As neither DUT-48 and DUT-46 show any phase transition with butane at this temperature, the question arises whether their frameworks can still undergo a structural contraction. A combined simulation and mechanical pressure study was performed on DUT-48 in parallel to the microcalorimetry experiments, which can be found in the paper published in collaboration with the TU Dresden, Chimie ParisTech and ICGM groups.<sup>(66)</sup> In brief, DFT optimisations of a single linker molecule under increasing stress show that buckling of the molecule is still possible, albeit at a much higher stress. Constant volume (N, V, T) molecular dynamics simulations of the evolution of the system free energy with decreasing unit cell volume have shown that, while a **cp** phase for DUT-48 exists, the increased tensile strength of the central backbone leads to an increase in both the free energy of this state and the activation energy required to enter it compared to DUT-49. To prove that structural transition can still take place, mercury intrusion experiments are carried out on both DUT-48 and DUT-49. The intrusion/extrusion curves on both materials show that an **op/cp** transition

## 5. Exploring novel behaviours

takes place, although with a much higher external pressure in the case of DUT-48 (65 MPa vs. 35 MPa). A similar approach on all other materials in this series reveals a very clear trend in both energy of the **cp** form and pressure required for the transition



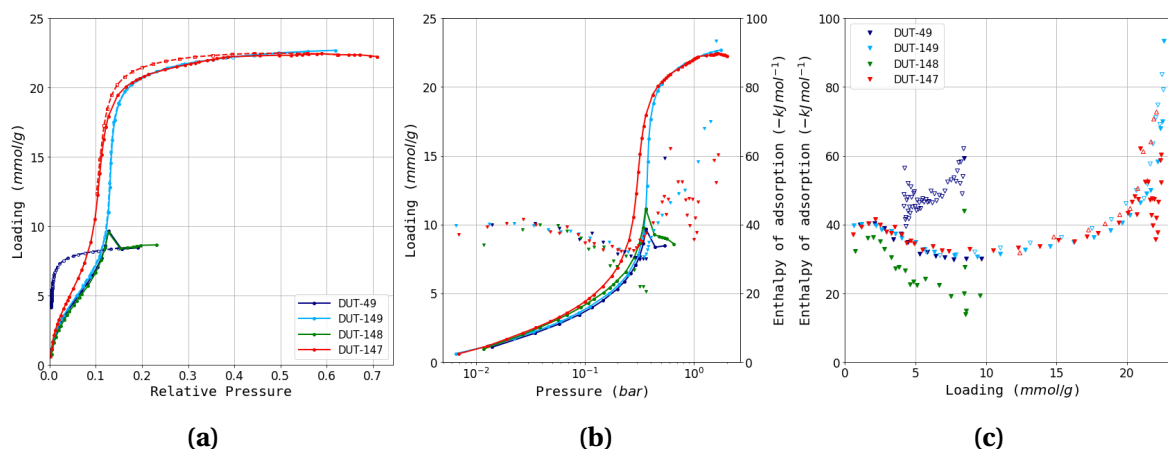
**Figure 5.7.:** The (a) isotherms and (b) enthalpy curves of the interpenetrated materials DUT-151 and DUT-152 as compared to DUT-49. Shaded regions are guides for the eye rather than uncertainty domains.

The interpenetrated materials DUT-151 and DUT-152 show a very different isotherm shape and enthalpy curve, as presented in Figure 5.7. In their case, the adsorption behaviour is very complex, with multiple transitions and hysteresis loops visible. However, several trends can still be rationalized. The total pore volume of DUT-152 is lower than that of DUT-151, as the bulkier central strut lowers the available space. Both materials show steeper adsorption curve at low pressures, due to the increased interactions of the adsorbate molecules with the doubled framework net. This is reflected in the differential adsorption enthalpy in the same region, with both DUT-151 and 152 displaying a higher enthalpy ( $45 kJ mol^{-1}$  to  $50 kJ mol^{-1}$  as opposed to  $40 kJ mol^{-1}$  for DUT-49). The smaller pore size of DUT-152 also leads to a shift in the adsorption isotherm to lower pressures and an increased enthalpy of adsorption at higher loadings. Finally, a total of three hysteresis loops are visible on DUT-152 associated with apparent transitions, highlighting several accessible intermediate pore states in its structure. These transitions are also found in the enthalpy curve, a result of different energetic contributions of the contraction/expansion. In order to elucidate such a complex interplay of factors more powerful methods such as *in-situ* PXRD are required to monitor the change of structural parameters during adsorption. While interesting, it should be pointed out that all transitions on DUT-151 and 152 seem to be continuous phase changes, with no

potential for an NGA-type contraction.

### Behaviour of “reinforced” linker analogues

A series of DUT-49 analogues, DUT-149, DUT-148 and DUT-147, with progressively connected central additions was created in order to observe the effect of linker strengthening on the structural transition. DUT-149 has two methyl groups in the ortho position relative to the central bond. DUT-148 has the same carbon number, but connects the two methyl groups with a single bond. Finally DUT-147 has a fully aromatic structure, with delocalised double bonds on each side of the original phenyl ring. The resulting isotherm and enthalpy curve are shown in Figure 5.8.



**Figure 5.8.:** (a) Experimental adsorption isotherms for DUT-49, DUT-149, DUT-148 and DUT-147. Enthalpy points are omitted for clarity. (b) A logarithmic plot of isotherms and enthalpy curves, to highlight the low pressure region. (c) Differential enthalpy of adsorption as a function of loading.

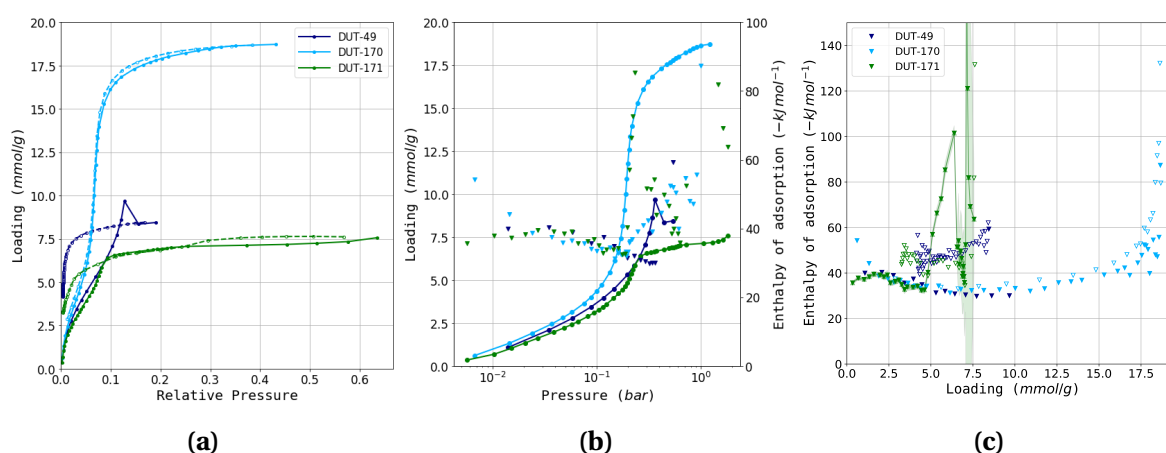
An unexpected trend emerges from the measured isotherms. DUT-149 does not show an NGA step, with adsorption taking place entirely on the **op** form of the material. In this regard it is an almost perfect non-flexible variant of DUT-49, with near-complete overlap of both its isotherm and enthalpy curves. A minute shift to lower pressure can be seen in the isotherm, as the methyl groups introduce a slight decrease in the large octahedral and medium tetrahedral pore size. Counterintuitively, the next material in the series, DUT-148, undergoes structural contraction in the same manner as DUT-49, retaining the NGA transition despite its increased connectivity. Finally, DUT-147 is stiffer and maintains its **op** state throughout adsorption. A slight wide hysteresis appears in the desorption branch, which may be an indication of subtle structural effects such as a rotation of the central part of the linker.

The different behaviour these analogues may have two possible causes: a change in the stability of the **cp** phase or a difference in the strain necessary to induce ligand buckling.

Both parameters are influenced by the introduced functionalisations. In the case of DUT-147 the central phenyl-phenyl bond has been strengthened, resulting in an increased strain required to induce the transition. For DUT-148 and DUT-149 the source of the counterintuitive trend is less clear-cut. In DUT-149, the methyl groups are sterically hindered, which results in the likely adoption of the lowest energy state, on each side of the central bond. This steric hindrance may increase the required strain to enter the elastic buckling regime. Conversely, the single bond in DUT-148 restricts the alkyl chain to a single side of the bond and may actually lower the energetic barrier for the existence of the **cp** form, through the stabilisation afforded by a chair-like 6-ring conformer. DFT optimisations, as those performed on the previous isorecticular linkers are recommended to shed light on the buckling behaviour.

### Behaviour of heterocyclic DUT-49 analogues

Using a thiophene-substituted aromatic linker may introduce additional guest-host interactions due to the resulting heterogeneous pore surface. Additionally, the change in geometry allows for new flexibility modes. The butane isotherms measured on these materials are summarized in Figure 5.9.



**Figure 5.9.:** (a) Experimental adsorption isotherms for DUT-49 and heterocyclic analogues DUT-170 and DUT-171. Enthalpy points are omitted for clarity. (b) A logarithmic plot of isotherms and enthalpy curves to highlight the low pressure region. (c) Differential enthalpy of adsorption as a function of loading, highlighting the adsorption branch and error range of DUT-171.

DUT-170, which has a linker with a similar structure and length as the naphthyl-derived DUT-48 is expected to remain non-flexible. This is seen to be the case, with the two isotherms similar in regard to total amount adsorbed and pore filling pressure. The isotherm of DUT-171 does show a structural transition, but without any observed NGA. A slight hysteresis can be seen, likely due to partial structure re-opening before the beginning of the desorp-

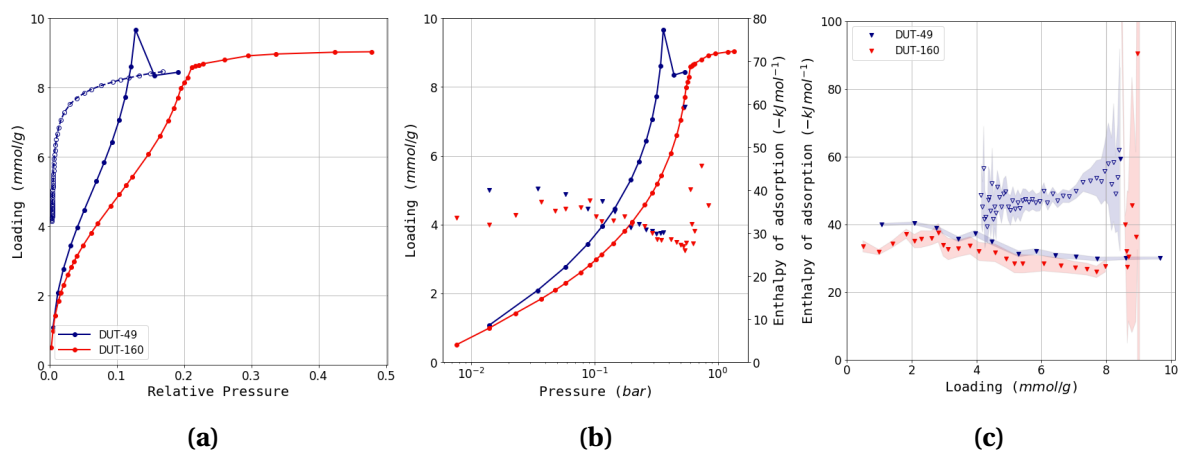
## 5. Exploring novel behaviours

tion branch. Instead of NGA, the enthalpy curve reveals a significant departure from the baseline as the slope of the isotherm changes slowly in a manner indicative of continuous contraction to a **cp** form. The resulting phase has enthalpies of desorption in the same range as DUT-49**cp**. This type of continuous phase change may suggest a different ligand deformation mechanism, without a sudden buckling and more akin to an elastic bending regime, perhaps due to the starting zig-zag shape of the linker.

Finally, the low pressure region of the enthalpy curve for DUT-170 shows a higher differential enthalpy of adsorption. However, a repeat of the experiment found that instead of a specific interaction of the heterocycle with the guest, this anomaly is due to poor thermal equilibration of the sample cell before the start of data recording in that particular measurement.

### Behaviour of elongated central strut materials

The final series of synthesised materials comprise DUT-160, 161 and 162, materials with a triple, double and single bond inserted between the central phenyl rings. Unfortunately, DUT-162 cannot be obtained in a desolvated open pore form, as it immediately collapses upon supercritical activation. Furthermore, the yield of DUT-160 and 161 was so low that not enough material was available for an experiment with DUT-161, and resulted in larger errors in the enthalpy curve of DUT-160. In particular the behaviour of DUT-161 could prove interesting, as the linker may exist in either a *trans* or *cis* isomer. The recorded isotherms are presented in Figure 5.10.



**Figure 5.10.:** (a) Experimental adsorption isotherms for DUT-49 and DUT-160. Enthalpy points are omitted for clarity. (b) A logarithmic plot of isotherms and enthalpy curves, to highlight the low pressure region. (c) Differential enthalpy of adsorption as a function of loading together with the uncertainty range for each measurement.

From its isotherm slope change in Figure 5.10a, DUT-160 can be seen to undergo a sharp

## 5. *Exploring novel behaviours*

transition at  $0.2 p/p_0$ , without NGA. The isotherm is very similar to the one measured on DUT-50, whose linker is comparable in length, pointing to a similar buckling behaviour. The lack of NGA is likely due to a lower energetic barrier between the **op** and **cp** state. The enthalpy curve of both DUT-160 and 50 has the same shape, although the differential enthalpy of adsorption on DUT-160 is lower across the entire loading range, a consequence of the larger uncertainty in the measurement.

### 5.4.3. An in-depth look at the NGA mechanism

## 5.5. Conclusion



## Bibliography

- [1] François-Xavier Coudert and Daniela Kohen. Molecular Insight into CO<sub>2</sub> “Trapdoor” Adsorption in Zeolite Na-RHO. *Chemistry of Materials*, 29(7):2724–2730, April 2017. ISSN 0897-4756, 1520-5002. doi: 10.1021/acs.chemmater.6b03837.
- [2] Yun Liu, Jae-Hyuk Her, Anne Dailly, Anibal J. Ramirez-Cuesta, Dan A. Neumann, and Craig M. Brown. Reversible Structural Transition in MIL-53 with Large Temperature Hysteresis. *Journal of the American Chemical Society*, 130(35):11813–11818, September 2008. ISSN 0002-7863, 1520-5126. doi: 10.1021/ja803669w.
- [3] Chen Zhang, Jason A. Gee, David S. Sholl, and Ryan P. Lively. Crystal-Size-Dependent Structural Transitions in Nanoporous Crystals: Adsorption-Induced Transitions in ZIF-8. *The Journal of Physical Chemistry C*, 118(35):20727–20733, September 2014. ISSN 1932-7447, 1932-7455. doi: 10.1021/jp5081466.
- [4] Simon Krause, Volodymyr Bon, Irena Senkowska, Daniel M. Többsen, Dirk Wallacher, Renjith S. Pillai, Guillaume Maurin, and Stefan Kaskel. The effect of crystallite size on pressure amplification in switchable porous solids. *Nature Communications*, 9(1), December 2018. ISSN 2041-1723. doi: 10.1038/s41467-018-03979-2.
- [5] Masashi Ito, Hirotomo Nishihara, Kentaro Yamamoto, Hiroyuki Itoi, Hideki Tanaka, Akira Maki, Minoru T. Miyahara, Seung Jae Yang, Chong Rae Park, and Takashi Kyotani. Reversible Pore Size Control of Elastic Microporous Material by Mechanical Force. *Chemistry - A European Journal*, 19(39):13009–13016, September 2013. ISSN 09476539. doi: 10.1002/chem.201301806.
- [6] Nicolas Chanut. *Using External Factors to Improve Gas Adsorption in Nanoporous Materials: Control of Humidity and Mechanical Pressure*. PhD thesis, Aix-Marseille, December 2016.
- [7] Thomas D. Bennett, Anthony K. Cheetham, Alain H. Fuchs, and François-Xavier Coudert. Interplay between defects, disorder and flexibility in metal-organic frameworks. *Nature Chemistry*, 9(1):11–16, December 2016. ISSN 1755-4330. doi: 10.1038/nchem.2691.
- [8] J. W. McBain and John Ferguson. On the Nature of the Influence of Humidity Changes upon the Composition of Building Materials. *The Journal of Physical Chemistry*, 31(4):564–590, January 1927. ISSN 0092-7325, 1541-5740. doi: 10.1021/j150274a010.
- [9] Gennady Y. Gor, Patrick Huber, and Noam Bernstein. Adsorption-induced deformation of nanoporous materials—A review. *Applied Physics Reviews*, 4(1):011303, March 2017. ISSN 1931-9401. doi: 10.1063/1.4975001.
- [10] B. P. Bering, O. K. Krasil'nikova, A. I. Sarakhov, V. V. Serpinskii, and M. M. Dubinin. Alteration of zeolite granule dimensions under krypton adsorption. *Bulletin of the Academy of Sciences of the USSR Division of Chemical Science*, 26(11):2258–2261, November 1977. ISSN 0568-5230, 1573-9171. doi: 10.1007/BF00958705.
- [11] G Reichenauer and G.W Scherer. Extracting the pore size distribution of compliant materials from nitrogen adsorption. *Colloids and Surfaces A: Physicochemical and Engineering Aspects*, 187-188:41–50, August 2001. ISSN 09277757. doi: 10.1016/S0927-7757(01)00619-7.
- [12] Susumu Kitagawa, Ryo Kitaura, and Shin-ichiro Noro. Functional Porous Coordination Polymers. *Angewandte Chemie International Edition*, 43(18):2334–2375, April 2004. ISSN 1433-7851, 1521-3773. doi: 10.1002/anie.200300610.
- [13] A. Schneemann, V. Bon, I. Schwedler, I. Senkowska, S. Kaskel, and R. A. Fischer. Flexible metal-organic frameworks. *Chem. Soc. Rev.*, 43(16):6062–6096, May 2014. ISSN 0306-0012, 1460-4744. doi: 10.1039/C4CS00101J.
- [14] Gérard Férey. Hybrid porous solids: Past, present, future. *Chem. Soc. Rev.*, 37(1):191–214, 2008. ISSN 0306-0012, 1460-4744. doi: 10.1039/B618320B.

## BIBLIOGRAPHY

- [15] Jian-Rong Li, Julian Sculley, and Hong-Cai Zhou. Metal–Organic Frameworks for Separations. *Chemical Reviews*, 112(2):869–932, February 2012. ISSN 0009-2665. doi: 10.1021/cr200190s.
- [16] Ritesh Haldar, Nivedita Sikdar, and Tapas Kumar Maji. Interpenetration in coordination polymers: Structural diversities toward porous functional materials. *Materials Today*, 18(2):97–116, March 2015. ISSN 13697021. doi: 10.1016/j.mattod.2014.10.038.
- [17] Ivo Stassen, Nicholas Burtch, Alec Talin, Paolo Falcaro, Mark Allendorf, and Rob Ameloot. An updated roadmap for the integration of metal-organic frameworks with electronic devices and chemical sensors. *Chemical Society Reviews*, 46(11):3185–3241, 2017. ISSN 0306-0012. doi: 10.1039/C7CS00122C.
- [18] L. Vanduyfhuys, S. M. J. Rogge, J. Wieme, S. Vandenbrande, G. Maurin, M. Waroquier, and V. Van Speybroeck. Thermodynamic insight into stimuli-responsive behaviour of soft porous crystals. *Nature Communications*, 9(1), December 2018. ISSN 2041-1723. doi: 10.1038/s41467-017-02666-y.
- [19] Christopher R. Murdock, Brianna C. Hughes, Zheng Lu, and David M. Jenkins. Approaches for synthesizing breathing MOFs by exploiting dimensional rigidity. *Coordination Chemistry Reviews*, 258-259:119–136, January 2014. ISSN 00108545. doi: 10.1016/j.ccr.2013.09.006.
- [20] Di Li and Katsumi Kaneko. Hydrogen bond-regulated microporous nature of copper complex-assembled microcrystals. *Chemical Physics Letters*, 335(1-2):50–56, February 2001. ISSN 00092614. doi: 10.1016/S0009-2614(00)01419-6.
- [21] Ryo Kitaura, Kenji Seki, George Akiyama, and Susumu Kitagawa. Porous Coordination-Polymer Crystals with Gated Channels Specific for Supercritical Gases. *Angewandte Chemie International Edition*, 42(4): 428–431, January 2003. ISSN 14337851, 15213773. doi: 10.1002/anie.200390130.
- [22] Ryo Kitaura, Kentaro Fujimoto, Shin-ichiro Noro, Mitsuru Kondo, and Susumu Kitagawa. A Pillared-Layer Coordination Polymer Network Displaying Hysteretic Sorption: [Cu<sub>2</sub>(pzdc)<sub>2</sub>(dpyg)]<sub>n</sub> (pzdc= Pyrazine-2,3-dicarboxylate; dpyg=1,2-Di(4-pyridyl)glycol). *Angewandte Chemie*, 114(1):141–143, January 2002. ISSN 0044-8249, 1521-3757. doi: 10.1002/1521-3757(20020104)114:1<141::AID-ANGE141>3.0.CO;2-D.
- [23] C. J. Kepert, T. J. Prior, and M. J. Rosseinsky. A Versatile Family of Interconvertible Microporous Chiral Molecular Frameworks: The First Example of Ligand Control of Network Chirality. *Journal of the American Chemical Society*, 122(21):5158–5168, May 2000. ISSN 0002-7863, 1520-5126. doi: 10.1021/ja993814s.
- [24] Andrew P. Nelson, Omar K. Farha, Karen L. Mulfort, and Joseph T. Hupp. Supercritical Processing as a Route to High Internal Surface Areas and Permanent Microporosity in Metal–Organic Framework Materials. *Journal of the American Chemical Society*, 131(2):458–460, January 2009. ISSN 0002-7863, 1520-5126. doi: 10.1021/ja808853q.
- [25] D. Fairen-Jimenez, S. A. Moggach, M. T. Wharmby, P. A. Wright, S. Parsons, and T. Düren. Opening the Gate: Framework Flexibility in ZIF-8 Explored by Experiments and Simulations. *Journal of the American Chemical Society*, 133(23):8900–8902, June 2011. ISSN 0002-7863, 1520-5126. doi: 10.1021/ja202154j.
- [26] Sandrine Bourrelly, Philip L. Llewellyn, Christian Serre, Franck Millange, Thierry Loiseau, and Gérard Férey. Different Adsorption Behaviors of Methane and Carbon Dioxide in the Isotypic Nanoporous Metal Terephthalates MIL-53 and MIL-47. *Journal of the American Chemical Society*, 127(39):13519–13521, October 2005. ISSN 0002-7863. doi: 10.1021/ja054668v.
- [27] C. Serre, S. Bourrelly, A. Vimont, N. A. Ramsahye, G. Maurin, P. L. Llewellyn, M. Daturi, Y. Filinchuk, O. Leynaud, P. Barnes, and G. Férey. An Explanation for the Very Large Breathing Effect of a Metal–Organic Framework during CO<sub>2</sub> Adsorption. *Advanced Materials*, 19(17):2246–2251, September 2007. ISSN 09359648, 15214095. doi: 10.1002/adma.200602645.
- [28] Tapas Kumar Maji, Ryotaro Matsuda, and Susumu Kitagawa. A flexible interpenetrating coordination framework with a bimodal porous functionality. *Nature Materials*, 6(2):142–148, February 2007. ISSN 1476-1122, 1476-4660. doi: 10.1038/nmat1827.
- [29] Y. Sakata, S. Furukawa, M. Kondo, K. Hirai, N. Horike, Y. Takashima, H. Uehara, N. Louvain, M. Meilikhov, T. Tsuruoka, S. Isoda, W. Kosaka, O. Sakata, and S. Kitagawa. Shape-Memory Nanopores Induced in Coordination Polymers. *Journal of the American Chemical Society*, 129(12):3648–3654, June 2007. ISSN 0002-7863, 1520-5126. doi: 10.1021/ja071807g.

## BIBLIOGRAPHY

- dination Frameworks by Crystal Downsizing. *Science*, 339(6116):193–196, January 2013. ISSN 0036-8075, 1095-9203. doi: 10.1126/science.1231451.
- [30] Mingyan Ma, Angélique Bétard, Irene Weber, Noura Saad Al-Hokbany, Roland A. Fischer, and Nils Metzler-Nolte. Iron-Based Metal–Organic Frameworks MIL-88B and  $\text{NH}_2$ -MIL-88B: High Quality Microwave Synthesis and Solvent-Induced Lattice “Breathing”. *Crystal Growth & Design*, 13(6):2286–2291, June 2013. ISSN 1528-7483, 1528-7505. doi: 10.1021/cg301738p.
- [31] Joobeom Seo, Ryotaro Matsuda, Hirotoishi Sakamoto, Charlotte Bonneau, and Susumu Kitagawa. A Pillared-Layer Coordination Polymer with a Rotatable Pillar Acting as a Molecular Gate for Guest Molecules. *Journal of the American Chemical Society*, 131(35):12792–12800, September 2009. ISSN 0002-7863, 1520-5126. doi: 10.1021/ja904363b.
- [32] Thierry Loiseau, Christian Serre, Clarisse Huguenard, Gerhard Fink, Francis Taulelle, Marc Henry, Thierry Bataille, and Gérard Férey. A Rationale for the Large Breathing of the Porous Aluminum Terephthalate (MIL-53) Upon Hydration. *Chemistry - A European Journal*, 10(6):1373–1382, March 2004. ISSN 0947-6539, 1521-3765. doi: 10.1002/chem.200305413.
- [33] Nicole Klein, Herbert C. Hoffmann, Amandine Cadiau, Juergen Getzschmann, Martin R. Lohe, Silvia Paasch, Thomas Heydenreich, Karim Adil, Irena Senkowska, Eike Brunner, and Stefan Kaskel. Structural flexibility and intrinsic dynamics in the  $\text{M}_2(2,6\text{-ndc})_2(\text{dabco})$  ( $\text{M} = \text{Ni}, \text{Cu}, \text{Co}, \text{Zn}$ ) metal–organic frameworks. *Journal of Materials Chemistry*, 22(20):10303, 2012. ISSN 0959-9428, 1364-5501. doi: 10.1039/c2jm15601f.
- [34] Gennady Yu. Gor and Alexander V. Neimark. Adsorption-Induced Deformation of Mesoporous Solids. *Langmuir*, 26(16):13021–13027, August 2010. ISSN 0743-7463, 1520-5827. doi: 10.1021/la1019247.
- [35] J.R. Dacey and M.J.B. Evans. Volume changes in saran charcoal caused by the adsorption of water, methanol and benzene vapours. *Carbon*, 9(5):579–585, October 1971. ISSN 00086223. doi: 10.1016/0008-6223(71)90079-0.
- [36] D. H. Bangham and Nazim Fakhoury. The Expansion of Charcoal accompanying Sorption of Gases and Vapours. *Nature*, 122(3079):681–682, November 1928. ISSN 0028-0836, 1476-4687. doi: 10.1038/122681b0.
- [37] G. Dolino, D. Bellet, and C. Faivre. Adsorption strains in porous silicon. *Physical Review B*, 54(24):17919–17929, December 1996. ISSN 0163-1829, 1095-3795. doi: 10.1103/PhysRevB.54.17919.
- [38] C. H. Amberg and R. McIntosh. A STUDY OF ADSORPTION HYSTERESIS BY MEANS OF LENGTH CHANGES OF A ROD OF POROUS GLASS. *Canadian Journal of Chemistry*, 30(12):1012–1032, December 1952. ISSN 0008-4042, 1480-3291. doi: 10.1139/v52-121.
- [39] Gerrit Günther, Johannes Prass, Oskar Paris, and Martin Schoen. Novel Insights into Nanopore Deformation Caused by Capillary Condensation. *Physical Review Letters*, 101(8), August 2008. ISSN 0031-9007, 1079-7114. doi: 10.1103/PhysRevLett.101.086104.
- [40] G Reichenauer and G.W Scherer. Nitrogen sorption in aerogels. *Journal of Non-Crystalline Solids*, 285(1-3): 167–174, June 2001. ISSN 00223093. doi: 10.1016/S0022-3093(01)00449-5.
- [41] Alexander V. Neimark, François-Xavier Coudert, Anne Boutin, and Alain H. Fuchs. Stress-Based Model for the Breathing of Metal–Organic Frameworks. *The Journal of Physical Chemistry Letters*, 1(1):445–449, January 2010. ISSN 1948-7185. doi: 10.1021/jz9003087.
- [42] Anne Boutin, François-Xavier Coudert, Marie-Anne Springuel-Huet, Alexander V. Neimark, Gérard Férey, and Alain H. Fuchs. The Behavior of Flexible MIL-53(Al) upon  $\text{CH}_4$  and  $\text{CO}_2$  Adsorption. *The Journal of Physical Chemistry C*, 114(50):22237–22244, December 2010. ISSN 1932-7447, 1932-7455. doi: 10.1021/jp108710h.
- [43] François-Xavier Coudert, Marie Jeffroy, Alain H. Fuchs, Anne Boutin, and Caroline Mellot-Draznieks. Thermodynamics of Guest-Induced Structural Transitions in Hybrid Organic-Inorganic Frameworks. *Journal of the American Chemical Society*, 130(43):14294–14302, October 2008. ISSN 0002-7863, 1520-5126. doi: 10.1021/ja805129c.

## BIBLIOGRAPHY

- [44] J Broekhoff. Studies on pore systems in catalysts IX. Calculation of pore distributions from the adsorption branch of nitrogen sorption isotherms in the case of open cylindrical pores A. Fundamental equations. *Journal of Catalysis*, 9(1):8–14, September 1967. ISSN 00219517. doi: 10.1016/0021-9517(67)90174-1.
- [45] Karena W. Chapman, Dorina F. Sava, Gregory J. Halder, Peter J. Chupas, and Tina M. Nenoff. Trapping Guests within a Nanoporous Metal–Organic Framework through Pressure-Induced Amorphization. *Journal of the American Chemical Society*, 133(46):18583–18585, November 2011. ISSN 0002-7863, 1520-5126. doi: 10.1021/ja2085096.
- [46] Jin Chong Tan and Anthony K. Cheetham. Mechanical properties of hybrid inorganic–organic framework materials: Establishing fundamental structure–property relationships. *Chemical Society Reviews*, 40(2): 1059, 2011. ISSN 0306-0012, 1460-4744. doi: 10.1039/c0cs00163e.
- [47] Isabelle Beurroies, Mohammed Boulhout, Philip L. Llewellyn, Bogdan Kuchta, Gérard Férey, Christian Serre, and Renaud Denoyel. Using Pressure to Provoke the Structural Transition of Metal–Organic Frameworks. *Angewandte Chemie International Edition*, 49(41):7526–7529, August 2010. ISSN 14337851. doi: 10.1002/anie.201003048.
- [48] Pascal G. Yot, Qintian Ma, Julien Haines, Qingyuan Yang, Aziz Ghoufi, Thomas Devic, Christian Serre, Vladimir Dmitriev, Gérard Férey, Chongli Zhong, and Guillaume Maurin. Large breathing of the MOF MIL-47(VIV) under mechanical pressure: A joint experimental–modelling exploration. *Chemical Science*, 3(4):1100, 2012. ISSN 2041-6520, 2041-6539. doi: 10.1039/c2sc00745b.
- [49] Richelle Lyndon, Kristina Konstas, Bradley P. Ladewig, Peter D. Southon, Prof Cameron J. Kepert, and Matthew R. Hill. Dynamic Photo-Switching in Metal–Organic Frameworks as a Route to Low-Energy Carbon Dioxide Capture and Release. *Angewandte Chemie*, 125(13):3783–3786, March 2013. ISSN 00448249. doi: 10.1002/ange.201206359.
- [50] Colin Dawson, Julian F. V. Vincent, and Anne-Marie Rocca. How pine cones open. *Nature*, 390:668, December 1997.
- [51] Mickael Boudot, Hervé Elettro, and David Grosso. Converting Water Adsorption and Capillary Condensation in Usable Forces with Simple Porous Inorganic Thin Films. *ACS Nano*, 10(11):10031–10040, November 2016. ISSN 1936-0851, 1936-086X. doi: 10.1021/acsnano.6b04648.
- [52] Christian Ganser, Gerhard Fritz-Popovski, Roland Morak, Parvin Sharifi, Benedetta Marmiroli, Barbara Sartori, Heinz Amenitsch, Thomas Griesser, Christian Teichert, and Oskar Paris. Cantilever bending based on humidity-actuated mesoporous silica/silicon bilayers. *Beilstein Journal of Nanotechnology*, 7:637–644, April 2016. ISSN 2190-4286. doi: 10.3762/bjnano.7.56.
- [53] Jarad A. Mason, Julia Oktawiec, Mercedes K. Taylor, Matthew R. Hudson, Julien Rodriguez, Jonathan E. Bachman, Miguel I. Gonzalez, Antonio Cervellino, Antonietta Guagliardi, Craig M. Brown, Philip L. Llewellyn, Norberto Masciocchi, and Jeffrey R. Long. Methane storage in flexible metal–organic frameworks with intrinsic thermal management. *Nature*, 527(7578):357–361, October 2015. ISSN 0028-0836, 1476-4687. doi: 10.1038/nature15732.
- [54] Hana Bunzen, Felicitas Kolbe, Andreas Kalytta-Mewes, German Sastre, Eike Brunner, and Dirk Volkmer. Achieving Large Volumetric Gas Storage Capacity in Metal–Organic Frameworks by Kinetic Trapping: A Case Study of Xenon Loading in MFU-4. *Journal of the American Chemical Society*, 140(32):10191–10197, August 2018. ISSN 0002-7863, 1520-5126. doi: 10.1021/jacs.8b04582.
- [55] Manuel Souto, Jorge Romero, Joaquín Calbo, Iñigo J. Vitórica-Yrezábal, José L. Zafra, Juan Casado, Enrique Ortí, Aron Walsh, and Guillermo Mínguez Espallargas. Breathing-Dependent Redox Activity in a Tetrathiafulvalene-Based Metal–Organic Framework. *Journal of the American Chemical Society*, August 2018. ISSN 0002-7863, 1520-5126. doi: 10.1021/jacs.8b05890.
- [56] A. C. McKinlay, J. F. Eubank, S. Wuttke, B. Xiao, P. S. Wheatley, P. Bazin, J.-C. Lavalley, M. Daturi, A. Vimont, G. De Weireld, P. Horcajada, C. Serre, and R. E. Morris. Nitric Oxide Adsorption and Delivery in Flexible

## BIBLIOGRAPHY

- MIL-88(Fe) Metal–Organic Frameworks. *Chemistry of Materials*, 25(9):1592–1599, May 2013. ISSN 0897-4756, 1520-5002. doi: 10.1021/cm304037x.
- [57] Patricia Horcajada, Christian Serre, Guillaume Maurin, Naseem A. Ramsahye, Francisco Balas, María Vallet-Regí, Muriel Sebban, Francis Taulelle, and Gérard Férey. Flexible Porous Metal–Organic Frameworks for a Controlled Drug Delivery. *Journal of the American Chemical Society*, 130(21):6774–6780, May 2008. ISSN 0002-7863, 1520-5126. doi: 10.1021/ja710973k.
- [58] Ulrich Stoeck, Simon Krause, Volodymyr Bon, Irena Senkowska, and Stefan Kaskel. A highly porous metal–organic framework, constructed from a cuboctahedral super-molecular building block, with exceptionally high methane uptake. *Chemical Communications*, 48(88):10841, 2012. ISSN 1359-7345. doi: 10.1039/c2cc34840c.
- [59] Simon Krause, Volodymyr Bon, Irena Senkowska, Ulrich Stoeck, Dirk Wallacher, Daniel M. Többsens, Stefan Zander, Renjith S. Pillai, Guillaume Maurin, François-Xavier Coudert, and Stefan Kaskel. A pressure-amplifying framework material with negative gas adsorption transitions. *Nature*, 532(7599):348–352, April 2016. ISSN 0028-0836. doi: 10.1038/nature17430.
- [60] Jana Schaber, Simon Krause, Silvia Paasch, Irena Senkowska, Volodymyr Bon, Daniel M. Többsens, Dirk Wallacher, Stefan Kaskel, and Eike Brunner. In Situ Monitoring of Unique Switching Transitions in the Pressure-Amplifying Flexible Framework Material DUT-49 by High-Pressure  $^{129}\text{Xe}$  NMR Spectroscopy. *The Journal of Physical Chemistry C*, 121(9):5195–5200, March 2017. ISSN 1932-7447, 1932-7455. doi: 10.1021/acs.jpcc.7b01204.
- [61] Jack D. Evans, Lydéric Bocquet, and François-Xavier Xavier Coudert. Origins of Negative Gas Adsorption. *Chem*, 1(6):873–886, December 2016. ISSN 24519294. doi: 10.1016/j.chempr.2016.11.004.
- [62] Jean Rouquerol, Stanislas Partyka, and Françoise Rouquerol. Calorimetric evidence for a bidimensional phase change in the monolayer of nitrogen or argon adsorbed on graphite at 77 K. *Journal of the Chemical Society, Faraday Transactions 1: Physical Chemistry in Condensed Phases*, 73:306, 1977. ISSN 0300-9599. doi: 10.1039/f19777300306.
- [63] Marcus Lange, Merten Kobalz, Jens Bergmann, Daniel Lässig, Jörg Lincke, Jens Möllmer, Andreas Möller, Jörg Hofmann, Harald Krautscheid, Reiner Staudt, and Roger Gläser. Structural flexibility of a copper-based metal–organic framework: Sorption of  $\text{C}_4$ -hydrocarbons and in situ XRD. *J. Mater. Chem. A*, 2(21): 8075–8085, 2014. ISSN 2050-7488, 2050-7496. doi: 10.1039/C3TA15331B.
- [64] Shyam Biswas, Tim Ahnfeldt, and Norbert Stock. New Functionalized Flexible Al-MIL-53-X ( $\text{X} = -\text{Cl}$ ,  $-\text{Br}$ ,  $-\text{CH}_3$ ,  $-\text{NO}_2$ ,  $-(\text{OH})_2$ ) Solids: Syntheses, Characterization, Sorption, and Breathing Behavior. *Inorganic Chemistry*, 50(19):9518–9526, October 2011. ISSN 0020-1669, 1520-510X. doi: 10.1021/ic201219g.
- [65] Pascal G. Yot, Ke Yang, Vincent Guillermin, Florence Ragon, Vladimir Dmitriev, Paraskevas Parisiades, Erik Elkaïm, Thomas Devic, Patricia Horcajada, Christian Serre, Norbert Stock, John P. S. Mowat, Paul A. Wright, Gérard Férey, and Guillaume Maurin. Impact of the Metal Centre and Functionalization on the Mechanical Behaviour of MIL-53 Metal–Organic Frameworks: Impact of the Metal Centre and Functionalization on the Mechanical Behaviour of MIL-53 Metal–Organic Frameworks. *European Journal of Inorganic Chemistry*, 2016(27):4424–4429, September 2016. ISSN 14341948. doi: 10.1002/ejic.201600263.
- [66] Simon Krause, Jack D. Evans, Volodymyr Bon, Irena Senkowska, Sebastian Ehrling, Ulrich Stoeck, Pascal G. Yot, Paul Iacomi, Philip Llewellyn, Guillaume Maurin, François-Xavier Coudert, and Stefan Kaskel. Adsorption Contraction Mechanics: Understanding Breathing Energetics in Isoreticular Metal–Organic Frameworks. *The Journal of Physical Chemistry C*, August 2018. ISSN 1932-7447, 1932-7455. doi: 10.1021/acs.jpcc.8b04549.

## A. Common characterisation techniques

pictures?

### A.1. Thermogravimetry

Thermogravimetry (TGA) is a standard laboratory technique where the weight of a sample is monitored while ambient temperature is controlled. Changes in sample mass can be correlated to physical events, such as adsorption, desorption, sample decomposition or oxidation, depending on temperature and its rate of change.

TGA experiments are carried out on approximately 15 mg of sample with a TA Instruments Q500 up to 800 °C. The sample is placed on a platinum crucible and sealed in a temperature controlled oven, under gas flow of 40 cm<sup>3</sup> min<sup>-1</sup>. Experiments can use a blanket of either air or argon. The temperature ramp can be specified directly and should be chosen to ensure that the sample is in equilibrium with the oven temperature and no thermal conductivity effects come into play. Alternatively, a dynamic “Hi-Res” mode can be used which allows for automatic cessation of heating rate while the sample undergoes mass loss.

The main purpose of thermogravimetry as used in this thesis is the determination of sample decomposition temperature, to ensure that thermal activation prior to adsorption is complete and that all guest molecules have been removed without loss of structure. To this end, experiments are performed under an inert atmosphere (argon), and the sample activation temperature is chosen as 50 °C to 100 °C lower than the sample decomposition temperature.

### A.2. Bulk density determination

Bulk density is a useful metric for the industrial use of adsorbent materials, as their volume plays a critical role in equipment sizing.

Bulk density is determined by weighing 1.5 ml empty glass vessels and settling the MOFs inside. Powder materials are then added in small increments and settled through vibration between each addition. The full vessel is finally weighed, which allowed the bulk density to

be determined. The same cell is used in all experiments, with cleaning through sonication between each experiment.

### A.3. Skeletal density determination

True density or skeletal density is determined through gas pycnometry in a MicrotracBEL BELSORP-max apparatus. Helium is chosen as the fluid of choice as it is assumed to be non-adsorbing.

The volume of a glass sample cell ( $V_c$ ) is precisely measured through dosing of the reference volume with helium up to ( $p_1$ ), then opening the valve connecting the two and allowing the gas to expand up to ( $p_2$ ). Afterwards approximately 50 mg of sample are weighed and inserted in a glass sample cell. After sample activation using the supplied electric heater to ensure no solvent residue is left in the pores, the same procedure is repeated to determine the volume of the cell and the adsorbent. With the volume of the sample determined, the density can be calculated by.

$$V_s = V_c + \frac{V_r}{1 - \frac{p_1}{p_2}} \quad (\text{A.1})$$

### A.4. Nitrogen physisorption at 77 K

Nitrogen adsorption experiments are carried out on a Micromeritics Triflex apparatus. Approximately 60 mg of sample are used for each measurement. Empty glass cells are weighed and filled with the samples, which are then activated in a Micromeritics Smart VacPrep up to their respective activation temperature under vacuum and then back-filled with an inert atmosphere. After sample activation, the cells are re-weighed to determine the precise sample mass. The cells are covered with a porous mantle which allows for a constant temperature gradient during measurement by wicking liquid nitrogen around the cell. Finally, the cells are immersed in a liquid nitrogen bath and the adsorption isotherm is recoded using the volumetric method. A separate cell is used to condense the adsorptive throughout the measurement for accurate determination of its saturation pressure.

### A.5. Vapour physisorption at 298 K

Vapour adsorption isotherms throughout this work are measured using a MicrotracBEL BELSORP-max apparatus in vapour mode. Glass cells are first weighed and then filled with

about 50 mg of sample. The vials are then heated under vacuum up to the activation temperature of the material and re-weighed in order to measure the exact sample mass without adsorbed guests. The cells are then immersed in a mineral oil bath kept at 298 K. To ensure that the cold point of the system occurs in the material and to prevent condensation on cell walls, the reference volume, dead space and vapour source are temperature controlled through an insulated enclosure.

## **A.6. Gravimetric isotherms**

The gravimetric isotherms in this thesis are obtained using a commercial Rubotherm GmbH balance. Approximately 1 g of dried sample is used for these experiments. Samples are activated in situ by heating under vacuum. The gas is introduced using a step-by-step method, and equilibrium is assumed to have been reached when the variation of weight remained below 30 µg over a 15 min interval. The volume of the sample is determined from a blank experiment with helium as the non-adsorbing gas and used in combination with the gas density measured by the Rubotherm balance to compensate for buoyancy.

## **A.7. High throughput isotherm measurement**

A high-throughput gas adsorption apparatus is presented for the evaluation of adsorbents of interest in gas storage and separation applications. This instrument is capable of measuring complete adsorption isotherms up to 50 bar on six samples in parallel using as little as 60 mg of material. Multiple adsorption cycles can be carried out and four gases can be used sequentially, giving as many as 24 adsorption isotherms in 24 h.<sup>(1)</sup>

## **A.8. Powder X-ray diffraction**

## **A.9. Nuclear magnetic resonance**

## **A.10. Adsorption manometry and calorimetry at 303 K**

## **Bibliography**

- [1] Andrew D. Wiersum, Christophe Giovannangeli, Dominique Vincent, Emily Bloch, Helge Reinsch, Norbert Stock, Ji Sun Lee, Jong-San Chang, and Philip L. Llewellyn. Experimental Screening of Porous Materials for



## *BIBLIOGRAPHY*

High Pressure Gas Adsorption and Evaluation in Gas Separations: Application to MOFs (MIL-100 and CAU-10). *ACS Combinatorial Science*, 15(2):111–119, February 2013. ISSN 2156-8952. doi: 10.1021/co300128w.

## D. Calculation of uncertainty in adsorption measurements

To obtain the experimental errors, the procedure described in the Guide to the Expression of Uncertainty in Measurement.<sup>(1)</sup> was used. The quantity, enthalpy or pressure, is first expressed as a function  $f(y)$  of other physical measured quantities through a functional relationship (Equation D.1). The standard uncertainty  $u_c(y)$  is then calculated on the basis of Equation D.2, where  $u_i(x_i)$  is the standard uncertainty in each input quantity. Here it is assumed that the input quantities are independent and uncorrelated. The error margins  $a_i$  for each quantity were taken from manufacturer specifications of the equipment used for recording. They were then divided by a value  $k_i$  chosen to cover the expected variance in that quantity, as each variable is assumed to be characterized by a probability distribution. The error introduced by the equation of state used (NIST REFPROP<sup>(2)</sup>) were assumed to be minor compared to the error introduced by the physical quantities, with the same to be said regarding the error in the calorimetric heat signal, which represents less than 1% of the error in enthalpy. Finally, the expanded uncertainty was calculated by choosing a suitable coverage factor of 1.645, corresponding to a 95% confidence interval.

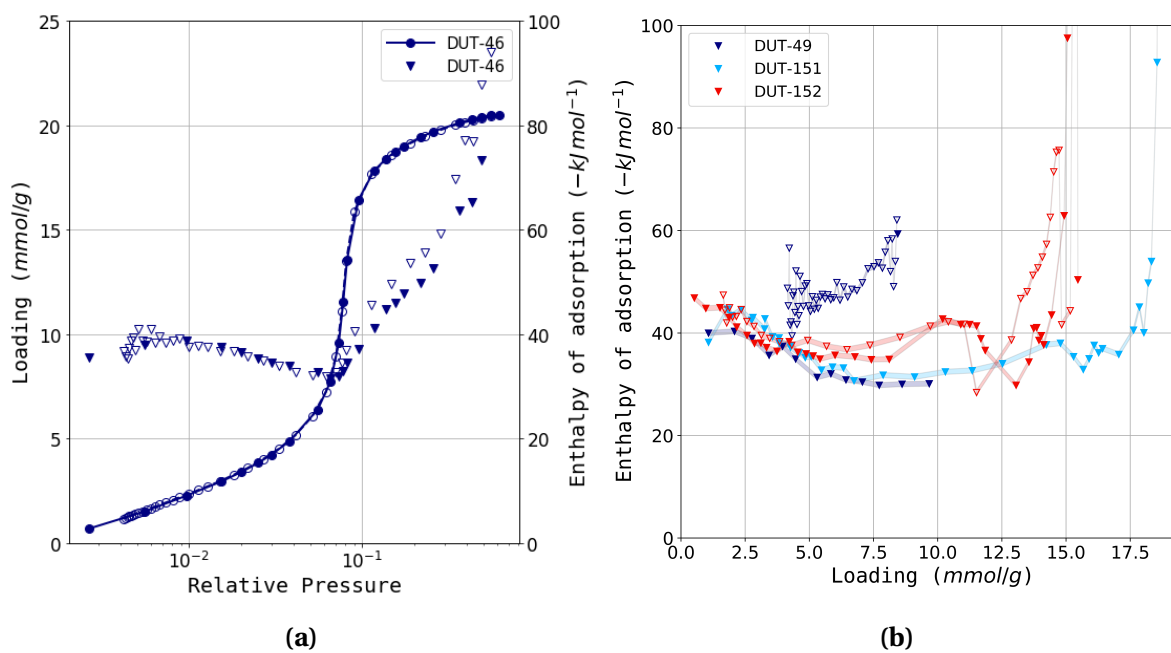
$$f(y) = f(N_1, N_2 \cdots N_i) \quad (\text{D.1})$$

$$u_c(y) = \sqrt{\sum_{i=1}^N \left( \frac{\partial f(y)}{\partial x_i} u_i x_i \right)^2} \quad (\text{D.2})$$

### Bibliography

- [1] Evaluation of measurement data — Guide to the expression of uncertainty in measurement. Technical Report 100:2008, JCGM, 2008.
- [2] Eric Lemmon. NIST Reference Fluid Thermodynamic and Transport Properties Database: Version 9.0, NIST Standard Reference Database 23, 1989.

## E. Appendix for chapter 5



**Figure E.1.:** The (a) isotherms and (b) enthalpy curves of the interpenetrated materials DUT-151 and DUT-152. Shaded regions are guides for the eye.

## Bibliography